Science of the Total Environment 958 (2025) 178140

Contents lists available at ScienceDirect

Science of the Total Environment

journal homepage: www.elsevier.com/locate/scitotenv

The risk of high-biomass HABs: Triggers and dynamics of a non-toxic bloom of *Prorocentrum micans* in Chilean Patagonia

Patricio A. Díaz [a,b,*], Leila Basti [c,d,e], Iván Pérez-Santos [a,f,g], Camila Schwerter [a], Osvaldo Artal [f,h], Sergio A. Rosales [i], Lauren Ross [j], René Garreaud [k,l], Carlos Conca [m,n], Gonzalo Álvarez [o,p,q,r], Zoë L. Fleming [s], Fabiola Villanueva [t], Manuel Díaz [u], Guido Mancilla-Gutiérrez [a], Robinson Altamirano [a], Camilo Rodríguez-Villegas [a], Pamela Urrutia [v], Geysi Urrutia [w], Pamela Linford [a,f], Tomás Acuña-Ruz [x], Rosa I. Figueroa [y]

[a] Centro i~mar, Universidad de Los Lagos, Casilla 557, Puerto Montt, Chile
[b] Centre for Biotechnology and Bioengineering (CeBiB), Universidad de Los Lagos, Casilla 557, Puerto Montt, Chile
[c] Faculty of Marine Environment and Resources, Tokyo University of Marine Science and Technology, 108-8477 Tokyo, Japan
[d] College of Agriculture and Veterinary Science, Department of Integrative Agriculture, United Arab Emirates University, Abu Dhabi, UAE
[e] WorldFish Headquarter, Jalan Batu Maung, Batu Maung, 11960 Bayan Lepas, Pulau Pinang, Malaysia
[f] Center for Oceanographic Research COPAS COASTAL, Universidad de Concepción, Chile
[g] Centro de Investigaciones en Ecosistemas de la Patagonia (CIEP), Coyhaique, Chile
[h] Departamento de Ingeniería en Obras Civiles, Facultad de Ingeniería y Ciencias, Universidad de La Frontera, Temuco, Chile
[i] Programa de Doctorado en Biología y Ecología Aplicada, Universidad Católica del Norte, Coquimbo, Chile
[j] Department of Civil and Environmental Engineering, University of Maine, Orono, ME, USA
[k] Centro de Ciencia del Clima y la Resiliencia (CR2), Universidad de Chile, Chile
[l] Departamento de Geofísica, Universidad de Chile, Santiago 8370449, Región Metropolitana, Chile
[m] Departamento de Ingeniería Matemática, Universidad de Chile, Santiago, Chile
[n] Centro de Biotecnología y Bioingeniería (CeBiB), Universidad de Chile, Santiago, Chile
[o] Facultad de Ciencias del Mar, Departamento de Acuicultura, Universidad Católica del Norte, Coquimbo 1281, Chile
[p] Centro de Investigación y Desarrollo Tecnológico en Algas (CIDTA), Facultad de Ciencias del Mar, Larrondo 1281, Universidad Católica del Norte, Coquimbo, Chile
[q] Center for Ecology and Sustainable Management of Oceanic Islands (ESMOI), Departamento de Biología Marina, Facultad de Ciencias del Mar, Universidad Católica del Norte, Coquimbo, Chile
[r] Centro de Innovación Acuícola AQUAPACIFICO, Larrondo 1281, Coquimbo, Chile
[s] Centro de Investigación en Tecnologías para la Sociedad, Facultad de Ingeniería, Universidad Del Desarrollo, Santiago, Chile
[t] @FAN Spa, Puerto Montt, Chile
[u] Programa de investigación Pesquera, Instituto de Acuicultura, Universidad Austral de Chile, Los Pinos s/n, Pelluco, Puerto Montt, Chile
[v] MOWI Chile, Puerto Montt, Chile
[w] Multi X, Av. Cardonal 2501, Puerto Montt, Chile
[x] Bloom Alert Spa, Santiago, Chile
[y] Centro Oceanográfico de Vigo, Instituto Español de Oceanografía (IEO-CSIC), Vigo, Spain

* Corresponding author at: Centro i~mar, Universidad de Los Lagos, Casilla 557, Puerto Montt, Chile
E-mail address: patricio.diaz@ulagos.cl (P.A. Díaz).

https://doi.org/10.1016/j.scitotenv.2024.178140
Received 16 July 2024; Received in revised form 26 November 2024; Accepted 13 December 2024
Available online 18 December 2024

HIGHLIGHTS

- HB-HABs caused by *Prorocentrum micans* are expanding to higher latitudes, making Chilean Patagonia particularly vulnerable to its blooms in the future.
- *P. micans* blooms in Chilean Patagonia seem to originate from a combination of hydrographic, land-based anthropogenic activities and climate change related factors.
- An eddy that persistently appears in the mean flow of the Gulf of Ancud could serve as a hotspot for the accumulation of HAB cells.
- *P. micans* HB-HABs can cause health and economic impacts, due to DMS production and mass mortalities in aquaculture farms, respectively.

GRAPHICAL ABSTRACT

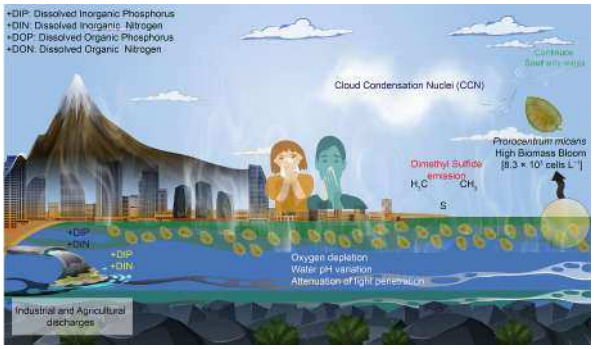

ARTICLE INFO

Editor: Daniel Wunderlin

Keywords:
Harmful algal blooms
High-biomass bloom
Prorocentrum micans
Dimethyl sulfide (DMS)
Human health
Southern Chile

ABSTRACT

Harmful algal blooms (HABs) of toxin-producing microalgae are recurrent in Patagonian fjord systems. Like toxigenic HABs, high-biomass harmful algal blooms (HB-HABs) have important socio-economic repercussions, but most studies have focused on the former. Here we report the formation and development of an intense HB-HAB of *Prorocentrum micans* that occurred in Northwest Chilean Patagonia in the late summer (February–March) of 2022. Concentrated and extensive brown spots were visible on the water surface, accompanied at the end of February by a strong odour. *Prorocentrum micans* cells were detected at relatively low densities (up to 215 cells mL^{-1}) in January but by February 11 cell densities exceeded 1000 cells mL^{-1}, reaching a maximum of 8.3×10^3 cell mL^{-1} in the surface layer. The high cell densities at Reloncaví Sound and the Gulf of Ancud were closely associated with narrow-ranging increases in the sea surface temperature (17–18.5 °C) and salinity (29–31 g kg^{-1}). Sentinel-2 satellite images from February 22 showed a colour change corresponding to the presence of the brown patches at both locations, consistent with the increases in the normalized index of chlorophyll differences (NDCI) and chlorophyll *a* concentrations (~50 μg L^{-1}). Satellite images from GHRSST indicated warmer waters in Reloncaví Sound and the Gulf of Ancud than in the Gulf of Corcovado, located 170-km to the south. An oceanographic 3-D model (MOSA) showed surface currents with a cyclonic eddy centred in the Gulf of Ancud. This circulation pattern suggested greater water retention in the study area during January and February, with the drifting and rotation of the coastal currents around the eddy maintaining the *P. micans* bloom. Thus, the elevated cell density of *P. micans* in the Gulf of Ancud, near the periphery of the eddy, confirm the presence of a material accumulation hotspot for HABs and HB-HABs.

1. Introduction

Harmful algal blooms (HABs), whether of toxin-producing microalgae or high-biomass (HB) species, occur globally and have serious economic repercussions for marine aquaculture, fisheries and tourism in addition to adverse effects on the environment and human health. In Chile, the increase in the incidence of HABs has been linked to climate change (Díaz and Figueroa, 2023; Díaz et al., 2023) and the development of aquaculture (Quiñones et al., 2019) but also to the increased monitoring of HAB and shellfish intoxications (Cabello and Godfrey, 2016; Díaz et al., 2019; Díaz et al., 2022). Among the HAB-forming taxa detected in Chile, the most frequently reported are species of diatoms and dinoflagellates. The latter include two species of *Prorocentrum* recorded by the national monitoring programmes and HAB databases: mainly *P. micans* but also *P. lima* (Barría et al., 2022; Cabello and Godfrey, 2016). Most of the approximately 137 species of *Prorocentrum* described thus far are marine cosmopolitan, unicellular, mixotrophic species with planktonic and epibenthic lifestyles and a capacity to form HB-HABs (Grzebyk et al., 1997; Hu et al., 1995; Jeong et al., 2010; Koike et al., 1998; Lin et al., 2014; Lu and Jeanette, 2001; Ndhlovu et al., 2017). In fact, outbreaks of planktonic species of *Prorocentrum* have been increasing globally, especially in estuarine and coastal marine environments (Glibert et al., 2005b; Gómez, 2005; Li et al., 2020), resulting in environmental damage and fisheries losses as the high algal biomass depletes oxygen availability, changes water acidity and significantly attenuates light penetration through the water column, thereby limiting photosynthesis and primary production in bloom areas (Glibert et al., 2005a; Glibert et al., 2012; Glibert et al., 2008; Heil et al., 2005; Pei et al., 2022). Moreover, some *Prorocentrum* species, in concert with *Dinophysis* spp., *Gonyaulax spinifera*, *Protoceratium reticulatum* and *Lingulodinium polyedrum*, produce highly bioactive toxins, including okadaic acid and its analogues, the dinophysistoxins (DSTs). The consumption of shellfish that have accumulated the toxins can result in potentially lethal diarrhetic shellfish poisoning (DSP), characterised by inflammation of the intestinal tract and diarrhoea (Díaz et al., 2022; Reguera et al., 2014).

Prorocentrum micans has served as the genus type (Hoppenrath et al., 2013) since *Prorocentrum* was recognised as a genus by Ehrenberg (1834). Blooms of this species are known to occur in three regions of Chile, including the Los Lagos region in Northern Patagonia, the site of 30 % of all microalgae blooms in Chile. Although not associated with the production of DSTs, *P. micans* is ichthyotoxic, accounting for 5 % of the microalgae-related fish mortality in Chilean salmon farms, with the remainder attributed to 24 species of harmful diatoms, silicoflagellates, raphidophytes, haptophytes and dinoflagellates (Barría et al., 2022). Several studies of HABs associated with toxin-producing species (Álvarez et al., 2011; Díaz et al., 2024a; Díaz et al., 2024b; Díaz et al., 2021) or with their ichthyotoxic effects on salmon farming (Baldrich

et al., 2024; Díaz et al., 2023; León-Muñoz et al., 2018) have been conducted in Chile; however, few studies have focussed on *Prorocentrum* blooms in particular.

Previous studies have shown that several of the most widespread HAB-forming species, including *Prorocentrum* spp. and, specifically. *P. minimum*, thrive in coastal areas enriched in dissolved inorganic phosphorus (DIP) and dissolved inorganic nitrogen (DIN), the levels of which have been projected to more than double by 2050 due to agricultural and industrial discharges (Dumont et al., 2005; Glibert et al., 2008; Glibert et al., 2005b; Harrison et al., 2005; Harrisson et al., 2005). Updated global modelling studies of phosphorus (P) and nitrogen (N) concentrations in coastal areas have shown a shift in the sources of those nutrients from 1985 to 2015 to 2015–2020, with natural sources declining, overwhelmed by the massive inputs resulting from land transformation, agriculture, sewage and aquaculture (e.g. Beussen et al., 2022).

DIP sources in Chilean waters are related to human sewage and P weathering, and DIN sources to sewage point sources, agricultural fertilizers and manure. However, concentrations of dissolved organic phosphorus (DOP) and dissolved organic nitrogen (DON) are lower in Chilean waters than in other coastal areas that host HABs, including those of *Prorocentrum* spp. (Beussen et al., 2022; Dumont et al., 2005; Harrison et al., 2005; Harrisson et al., 2005).

Apart from nutrients, other factors might be enhancing *Prorocentrum* blooms. For example, over the last four decades, the combined effects of increased greenhouse gas concentrations and ozone depletion in the polar stratosphere have resulted in an intensification of the subtropical high over the SE Pacific and a poleward shift of the westerly wind belt (e.

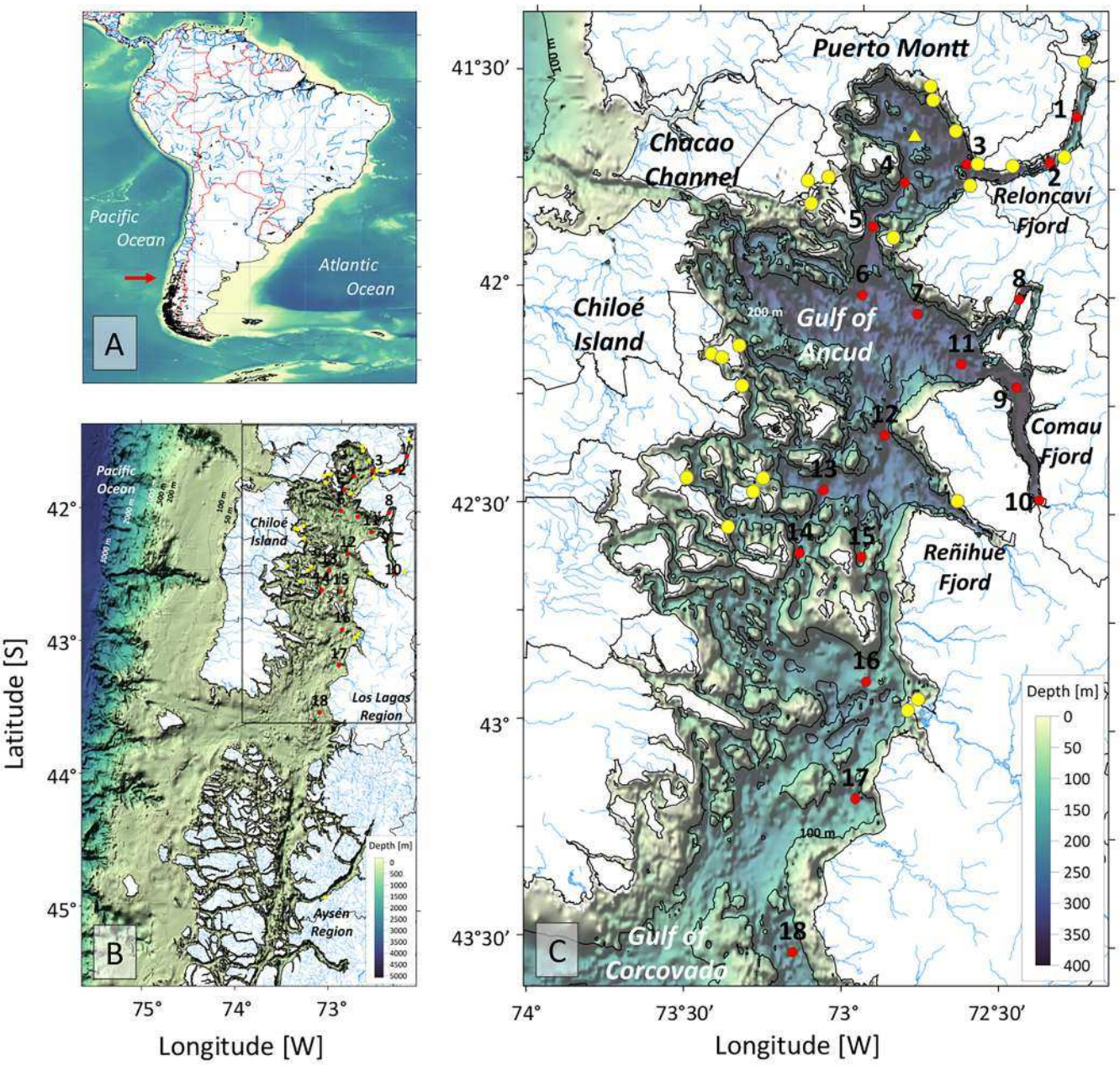

Fig. 1. Maps showing the study area. A) South America (red arrow indicates the NW Patagonia; B) The inland sea of NW Patagonia (black box indicates the Chiloé inland sea); C) the Chiloé inland sea, including Reloncaví Sound and Reloncaví Fjord. Black circles show the locations of the salmon farms where phytoplankton data were obtained, and red circles the location of the 18 sampling stations visited during the oceanographic cruise from the head of Reloncaví Fjord to the Gulf of Corcovado. The yellow triangle at the centre of Reloncaví Sound denotes the position of the i ~ mar oceanographic buoy.

g., Polvani et al., 2011). These large-scale changes project onto the positive phase of the Southern Annular Mode (SAM; Fogt and Marshall, 2020) and in NW Patagonia explain the recent trends of less precipitation, enhanced southerly winds and increased solar radiation—most markedly during the austral summer and fall months (e.g., Garreaud, 2018)—superimposed on the region's natural climate variability (El Niño and Southern Oscillation [ENSO] cycle). These shifts in climate together with anthropogenic factors may favour blooms of some species of HABs over those of others.

Coastal circulation and transport patterns were also considered as potential bloom enhancers. Previous studies showed that, in regions with a complex coastal geomorphology, such as Northern Patagonia, the currents can be steered by the topographic variability of the coastline, thus elevating vorticity (Zimmerman, 1978). The resulting circular velocity patterns ('eddies') worsen coastal HAB events by limiting water transport (Quin and Shen, 2019) and augmenting microalgal growth by advecting nutrients to the surface (Coria-Monter et al., 2017). Thus, our study combined in-situ collected water quality and microalgae cell density data, satellite altimetry and coastal simulations of circulation patterns as well as Langrangian particle tracking in the interconnected fjord, gulfs and sounds of Northern Patagonia in order to identify and characterise the environmental drivers that led to a massive bloom of *P. micans* in NW Chilean Patagonia in the summer of 2022. Finally, we discuss our findings in a global context, as a guide to understanding and predicting the adverse effects of HABs.

2. Materials and methods

2.1. Study area

The study was conducted in the area encompassing Reloncaví Fjord and Reloncaví Sound and the inner sea of Chiloé Island (referred to hereafter as the Chiloé inland sea), from the Gulf of Ancud to the Gulf of Corcovado (41.5°S–43.5°S; Fig. 1). This area forms part of the channel system of NW Patagonia, which is characterised by a complex coastal morphology, large bathymetric gradients (up to 450 m at the mouth of Reloncaví Fjord) and an irregular shoreline, all of which influence the circulation of oceanic water (Pickard, 1971). The bathymetric features in the northern Patagonian fjords and channels have several shallow constriction-sills (0.5–10 km wide; 50–100 m depth), which segment the bathymetry forming isolated deep micro-basins (200–1300 m) impeding the deep-water renewal (Schneider et al., 2014) and causing hypoxia (Linford et al., 2023; Silva and Vargas, 2014). The bathymetric information used in the study area map (Fig. 1) were obtained from the GEBCO 2023 grided data (https://download.gebco.net/, access on 19 August of 2023).

The salinity gradient in the upper 50 m of the water column ranges from 27 to 33 g kg^{-1} and is primarily determined by seasonal rainfall (Pérez-Santos et al., 2021; Pickard, 1971; Silva et al., 1995). The mean total annual rainfall recorded at the meteorological station at Tepual airport in Puerto Montt (41.4°S, 73.1°W), the northern gate to Patagonia, between 1961 and 2022 was 1650 mm per year, but with a significant trend of a ~100-mm reduction per decade (Boisier et al., 2019; Díaz and Figueroa, 2023). During the austral summer, the poleward shift of the westerlies and the expansion of the subtropical high cause a decline in precipitation and an increase in southerly winds, in contrast to the situation during the austral winter.

The Desertores Islands are one of the main geographic features of the study area, as they contribute to the transport and exchange of water masses within the Chiloé inland sea, in particular the exchange of freshwater between the Gulf of Ancud and the Gulf of Corcovado (Strub et al., 2019).

2.2. Regional climate and local meteorological conditions

Data on local meteorological conditions were obtained from Tepual station, operated by the Chilean Weather Service and located at Puerto Montt Airport, just north of Reloncaví Sound. The analysis was extended using gridded (0.05° × 0.05° lat-lon) precipitation and temperature fields over Chile from 1979 to date, obtained from the CR2Met dataset, which merges observations and reanalysis data (Álvarez-Garreton et al., 2018). Large-scale atmospheric conditions were described using the monthly means of sea level pressure (SLP) and the geopotential height at selected pressure levels from the fifth-generation ECMWF reanalysis (ERA5; Hersbach et al., 2020), available from 1948 onwards, on a 0.25° × '0.25° latitude-longitude grid (Kalnay et al., 1996). Monthly mean ENSO and SAM indexes were obtained from the National Oceanographic Administration's Physical Science Laboratory.

Meteorological data (total precipitation, relative humidity, air temperature, solar radiation, wind velocity and direction) as well as sea level and current measurements were obtained from the i ~ mar Oceanographic Centre buoy (41°38.183′ S–72°50.069′ W) (Fig. 1). Affixed to the buoy are a meteorological station (Gill GMX500), a conductivity-temperature-depth probe (CTD AML model Metrec-XL) and an acoustic Doppler current profiler (ADCP AWAC 400 kH).

2.3. Field sampling

2.3.1. Monitoring of phytoplankton at salmon farms

Data on *P. micans* cell density collected at several sampling stations positioned within salmon farms along the coast of the inner sea of the Los Lagos region (Fig. 1) were obtained from the Salmonid Oceanographic and Environmental Program (POAS: *Programa Oceanografico y Ambiental en Salmonidos*) from January 1 to March 31, 2022. Under the framework of this program, Niskin bottles (5 L) were used to collect water samples from four depths (0, 5, 10, 15 m) for quantitative analyses of *P. micans* cells. The samples were fixed with Lugol's iodine solution (0.5–1 % final concentration) (Lovegrove, 1960).

For quantitative analyses of *P. micans* cells, 10 mL of the unconcentrated, acidic, Lugol's-fixed samples were left to sediment overnight before they were analysed under an inverted microscope (Olympus CKX41) using the method described in Utermöhl (1958). The whole surface of a 10-mL sedimentation chamber was scanned, so the detection level was 100 cells L^{-1} (i.e., one cell detected after examination of the entire surface of the sedimentation chamber base-plate). Cells of *P. micans* were identified to the species level following taxonomic guides (Mardones and Clément, 2016; Tomas, 1997).

2.3.2. Monitoring of hydrographic conditions at a fixed sampling station

Sampling for measurements of physical and biological parameters was carried out monthly from December 2021 to April 2022, in Reloncaví Sound, northern Patagonia. The data were collected from the fixed position of the oceanographic buoy operated by the i ~ mar Centre (Fig. 1).

Vertical profiles of temperature, salinity, DO and fluorescence (a direct proxy for chlorophyll-*a* [Chl-*a*]) were obtained monthly at depths of 0–240 m at a sampling rate of 24 Hz using an AML (model Metrec-XL) oceanographic CTD (www.amloceanographic.com). Temperature and salinity data from the CTD were converted to conservative temperature (°C) and absolute salinity (SA, in g kg^{-1}) according to the thermodynamic equations of seawater 2010 (IOC et al., 2010). The CTD data were processed using the software provided by the manufacturer and visualised using Ocean Data View software (Schlitzer, 2015).

Water samples for inorganic nutrient analysis were collected at fixed depths (0, 5, 10, 25 and 50 m) using a 5-L Niskin bottle. Dissolved inorganic nutrients (NO_3^-, NO_2^-, PO_4^{3-} and Si $(OH)_4$) were analysed from 15-mL seawater samples, previously stored at −20 °C in HDPE bottles, using a Seal AA3 AutoAnalyzer according to the methodology described in Grasshoff et al. (1983) and the standard methods for seawater analysis (Kattner and Becker, 1991). Ammonia analyses were omitted for logistical reasons, as in the remote areas of Southern Chile it was essentially impossible to ensure determinations of this labile molecule within the

recommended 6 h limit or recommended 24 h timeframe after sample collection.

Water samples for analyses of *P. micans* cell density were collected from six discrete depths (0, 5, 10, 15, 25, 50 m) using 5-L Niskin bottle. Their fixation, storage and analysis are described in Section 2.3.1.

2.3.3. Oceanographic cruise during the bloom

An oceanographic research cruise of the *R.V. Jurgen Winter* in the Chiloé inland sea was conducted during late summer of 2022, from February 15 to March 5. During the cruise, samples were collected at 18 sampling stations along a 420-km transect (Fig. 1). The transect began at the head of Reloncaví Fjord (station 1), passing through Reloncaví Sound (stations 3–5) and the Gulf of Ancud, where it entered Comau Fjord (stations 8–10), then returning to the Gulf of Ancud (stations 11–12) (Fig. 1C) and finally passing through Apiao Channel (station 14), ending in the Gulf of Corcovado (station 18).

Vertical profiles of temperature, salinity and in vivo Chl-*a* fluorescence were obtained at each sampling station, from the surface to the bottom, using an AML Oceanographic CTD profiler model Metrec-XL as described in Section 2.3.2. Surface water samples for cell density analysis of *P. micans* were collected at each station using a 5-L Niskin bottle. At stations 1 (head of Reloncaví Sound), 7 (Gulf of Ancud) and 18 (Gulf of Corcovado), higher spatial resolution sampling was carried out. At these stations water samples were collected every 2 m, from the surface to 20 m depth, and then at depths of 25 m and 30 m. The samples were fixed and stored as described in Section 2.3.1.

2.4. Satellite images

High-resolution (10 m) Sentinel-2 images were obtained between February 10 and March 10, 2022 from the Copernicus open-access hub to provide complementary evidence of the locations and extent of algal abundance determined during the field campaigns. The images were projected in the system under the reference EPSG:32718 - WGS 84/UTM zone 18S. Natural colour bands were obtained by combining the red (B4), green (B3) and blue (B4) bands using a gamma value of 0.3 to better visualise each image. In addition, the normalized difference chlorophyll index (NDCI) was estimated according to the following equation (Mishra and Mishra, 2012):

$$NDCI = \frac{(Rrs705 - Rrs665)}{(Rrs705 + Rrs665)}$$

where Rrs705 is the remote sensing reflectance at 705 nm (visible and near-infrared NIR) and Rrs665 is the remote sensing reflectance at 665 nm (red).

The Chl-*a* concentration was estimated according to the OC3 algorithm (O'Reilly and Werdell, 2019):

$$log_{10}Chla = \sum_{i=0}^{4} a_i X^i$$

where:

a_i coefficients were obtained from Pahleva et al. (2020):

$$X = log_{10}\frac{max(Rs442, Rs492)}{Rs560}$$

Rrs442 = remote sensing reflectance at 442 nm (Coastal Aerosol)

Rrs492 = remote sensing reflectance at 492 nm (Blue)

Rrs560 = remote sensing reflectance at 492 nm (Green)

Daily satellite recordings of sea surface temperature (SST) were obtained from the level 4 product from the Group for High Resolution Sea Surface Temperature (GHRSST) (Beggs et al., 2023) (https://www.ghrsst.org/), which has a resolution of 1 km. The images were obtained from two SST time series (Reloncaví Sound and Gulf of Ancud).

2.5. Modelling

Data on surface currents between January and April of 2022 were obtained from the Chilean Patagonia oceanic forecasting model (MOSA) (Ruiz et al., 2021). This oceanographic 3-D model has been operational since 2017; it is based on the Coastal and Regional Ocean Community Model (CROCO, Debreu et al., 2012) and was developed by the Fisheries Development Institute (IFOP website: www.ifop.cl). In previous studies carried out in NW Patagonia, MOSA had a satisfactory response to seasonal variabilities in temperature, salinity and currents (Bedriñana-Romano et al., 2023; Mardones et al., 2023; Ruiz et al., 2021). All variables of MOSA are hourly and have a spatial resolution of 1 km, distributed over 42 vertical levels that follow the area topography. Forecasts for the last week of MOSA can be found on the oceanographic observing system CHONOS (Reche et al., 2021). Specifically, currents were analysed using surface data from the first 24 h of each daily forecast generated between January 1 and April 30, 2022 and covering the study area. Daily and weekly averages for these numerical outputs were then calculated and the average circulation over the entire study period was determined.

2.6. Particle dispersion modelling

Lagrangian particle tracking experiments using the OpenDrift model (Dagestad et al., 2018) were carried out to track the spatial-temporal evolution of surface-released particles in the Chiloé inland sea, as a proxy for microalgal transport. OpenDrift is an open-source, generic, modular Lagrangian particle tracking model under development at the Norwegian Meteorological Institute, with contributions from the wider scientific community (https://opendrift.github.io). The model has been used to evaluate the spatial and temporal dynamics of HAB events along Chilean coasts (Rosales et al., 2024). In this study, two 30-day particle release experiments were conducted. The first experiment commenced on February 8, 2022 (preceding the event), and the second on February 23, 2022 (during the event). In each one, 1000 random particles were released from the surface within a 600-m radius centred at the mouth of Reloncaví Fjord (41.7225°S; 72.6505°W), where the bloom was expected to start. In these simulations, the inert particles were considered to lack mass or size and to be unresponsive to environmental conditions. Consequently, they were not destroyed or extinguished upon interacting with variables such as density, salinity or temperature. However, the particles were able to move within the vertical water column in response to vertical currents and bathymetry. Additionally, each particle that reached the coast was capable of recirculating if the tides or currents permitted. Zonal, meridional and vertical currents for the particle tracking period were extracted from the operational oceanographic forecast MOSA to force the Opendrift model.

2.7. Data analysis

A generalized linear model (GLM) with a log link function and negative binomial distribution (McCullagh and Nelder, 1989) was implemented to evaluate the influence of different environmental factors on the prevalence of superficial density of *P. micans* in the study area. The explanatory variables were temperature, salinity, dissolved oxygen, pH, and turbidity. Homoscedasticity was tested in a Levene's test, and collinearity in a variance inflation test (VIF), using a threshold VIF $\leq$4 (Fox and Weisberg, 2011). Even when, Chl-*a* showed collinearity with the other predictor variables, due to its importance for explain *P. micans* distribution in the study area it was included in the GLM model. To avoid any confusion in this regard, we use Akaike criteria (Akaike, 1974) to compare the model with and without Chl-*a* and the differences between this models was AIC $<$ 1.5. Only main effects were included in the model and explanatory variable effects were determined using a X^2 marginal test type II ANOVA (Venables and Ripley, 2013). Finally, positive/negative values of the β-coefficients (Table S1) were

used to infer if the associated predictor variable has a positive/negative relationship with the *P. micans* cell density. The level of significance for each model was set to $\alpha = 0.05$.

3. Results

3.1. Global and local climate contexts

Fig. 2A shows the daily precipitation and maximum air temperature at station Tepual for the period January 1 to March 31, 2022. From the first week of January to mid-February, precipitation events were few and weak, causing a precipitation deficit of about 20 % during these two months. Precipitation was more frequent the last week of February and near average during March. However, the dry conditions during January–February were linked with an abnormal extension of the SE Pacific high pressure cell into western Patagonia (Fig. 2B) that caused persistent southerly winds in the study area. Later, the anticyclone retracted northward, resulting in more prevalent westerly winds at low levels (Fig. 2C) and the arrival of frontal perturbations in NW Patagonia. The maximum temperature was ~1 °C above the historical average for late summer, including two warm events (>27 °C), on January 27 and February 22. According to the CR2Met dataset, the aforementioned features in Puerto Montt also occurred in the rest of NW Patagonia. The dry, anticyclonic conditions in this region were consistent with the positive phase of the SAM during January–February 2022, as inferred from the sea level pressure anomalies shown in Fig. S1A. The SAM index during these two months was +0.7, in line with the positive tendency it has followed for the last few decades. By contrast, in the tropical Pacific and along much of the coast of South America, negative SST anomalies occurred that were consistent with the La Niña conditions that prevailed at that time (Fig. S1B). Note that insignificant SST anomalies prevailed off the coast of NW Patagonia.

Based on the in-situ measurements at the i ~ mar buoy, southerly winds were dominant from mid-February through most of March over Reloncaví Sound, with a maximum velocity of 5 m s^{-1} between March 13 and 18, 2022 (Fig. 3A). During the same period, the relative humidity fluctuated between 40 % and nearly 100 % (Fig. 3B). The lowest relative humidity (40 %) coincided with the highest air temperature (24 °C), both recorded between February 21 and 23, 2022 (Fig. 3C). Subsequently, the temperature was characterised by a large diurnal variability, although with a clear decreasing trend, with values close to 8 °C reached at the end of March 2022, during the transition from austral summer to fall (Fig. 3C). Finally, the solar radiation followed the classic pattern of a diurnal increase towards local midday, reaching maximum values close to 1000 W m^{-2} during the second half of February and early March (Fig. 3D).

3.2. Prorocentrum micans bloom

A dense bloom of the dinoflagellate *P. micans* occurred in NW Patagonia during the austral summer of 2022. A stark brown biomass developed on the water surface at Reloncaví Sound and the Gulf of Ancud (Fig. 4A–C) that appeared as fronts in coastal areas surrounding salmon farming centres (Fig. 4C).

Phytoplankton data from the salmon farming monitoring programme in Reloncaví Sound provided evidence of the persistence of the bloom

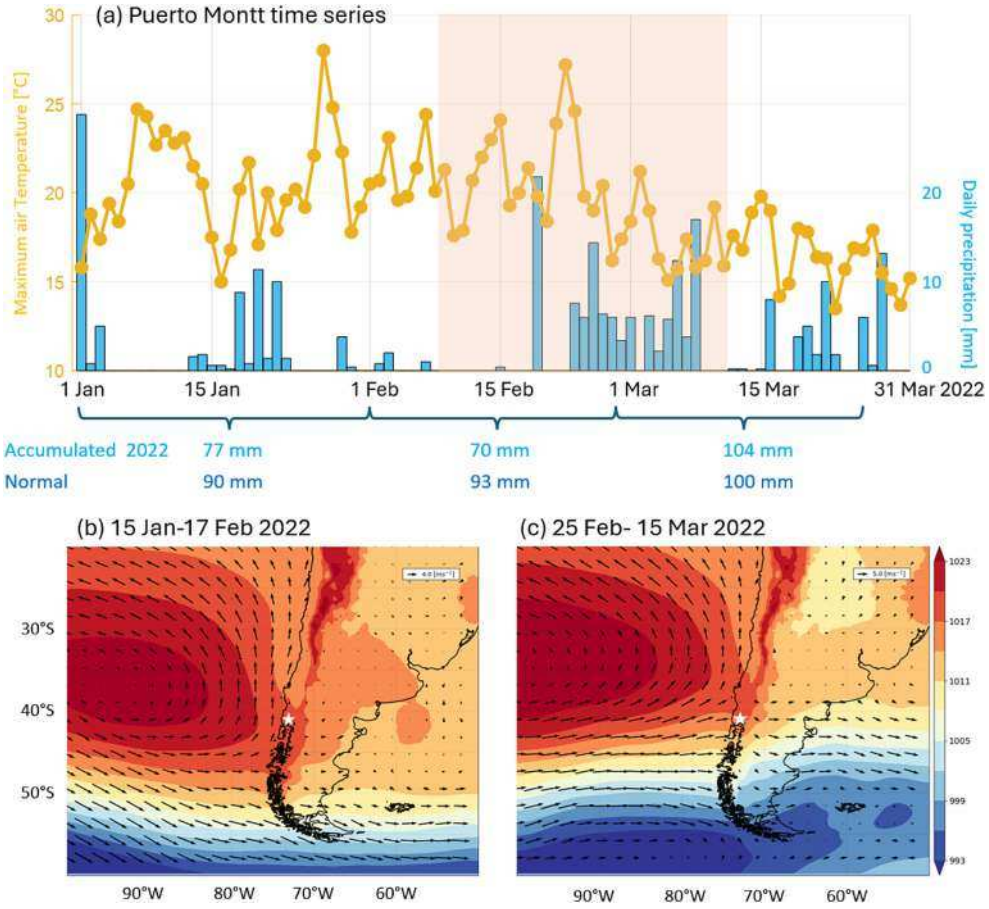

Fig. 2. A) Daily series of maximum air temperature (yellow line) and precipitation (blue bars) at Tepual Airport, Puerto Montt. The monthly accumulations for 2022 and the historical accumulations are shown below the graph. B) Mean sea level pressure (colours) and surface winds (arrows) for the period January 15–February 17, 2022. (c) Same as (b) for the period February25–March 15, 2022.

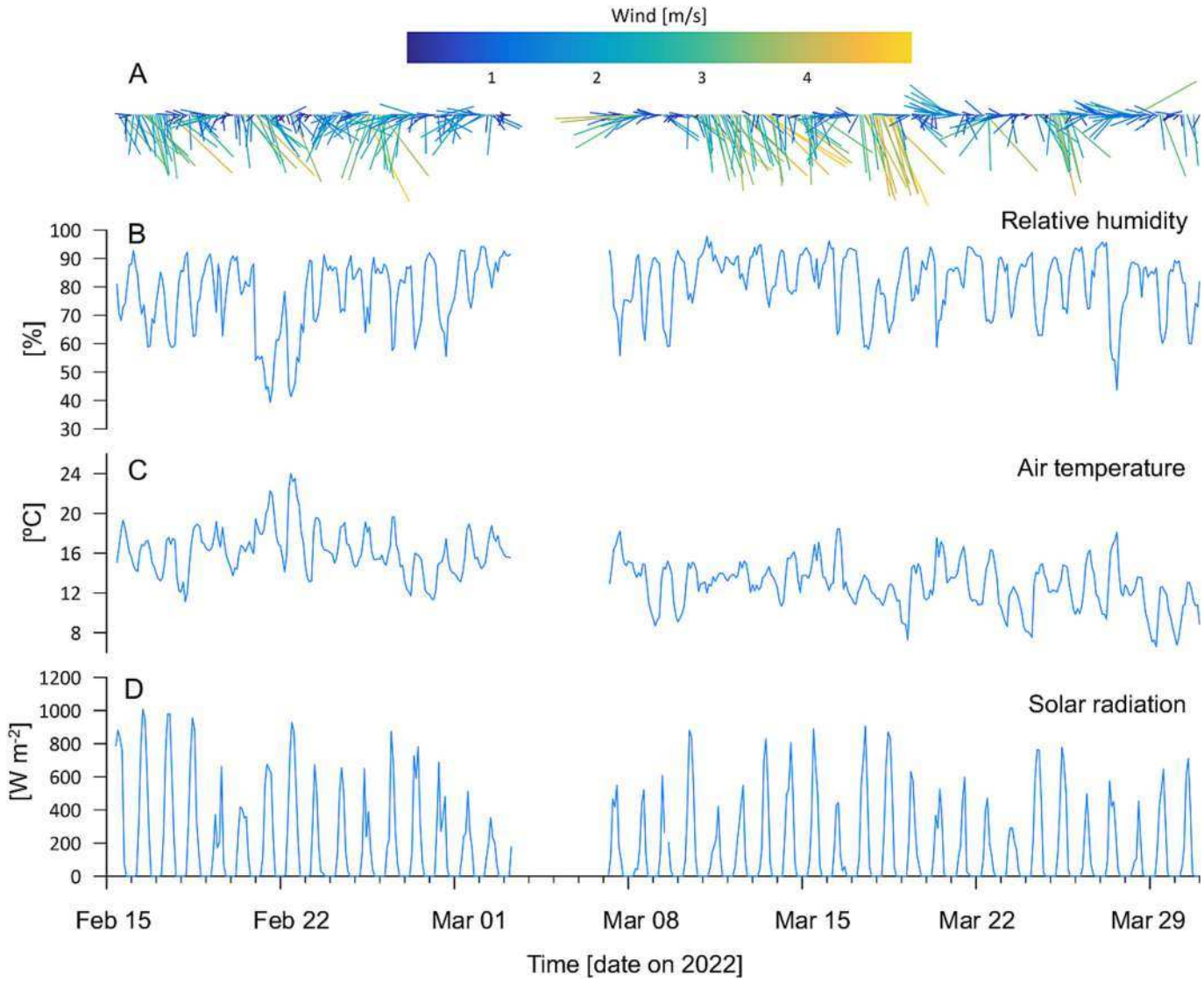

Fig. 3. Time series of A) wind direction and velocity (m s^{-1}), shown in a vector diagram (negative values correspond to southerly winds); B) relative humidity (%); C) air temperature (°C) and D) solar radiation (W m^{-2}). The data were recorded hourly at the i ~ mar oceanographic buoy from February 15 to March 31, 2022.

from February 10 to March 10, 2022 (Fig. 4E-G). High cell densities of *P. micans* were detected at the three surface layers (0, 5 and 10 m), with the highest cell density (>8.3 × 10^3 cells mL^{-1}) occurring on February 24 (Fig. 4E). High cell densities (> 6.8 × 10^3 cells mL^{-1}) were detected at 10 m depth one week earlier, on February 17, 2022 (Fig. 4G).

3.3. Oceanographic conditions at i ~ mar buoy

Data from the oceanographic buoy evidenced two characteristics of the surface layer during the sampling period (austral summer): from February 4 to 24, 2022, warmer (16°-20 °C), less salty (25–30 PSU), oxygenated-oversaturated water (8–12 mg L^{-1}, 100–130 % saturation), and from February 25 to March 30, 2022, colder (12°-15 °C), saltier (28–32 PSU) water with depleted levels of DO (3–8 mg L^{-1}, 40–100 % saturation) (Fig. 5A–C). Chl-*a* concentrations were higher during the *P. micans* bloom, reaching a maximum of 50 μg L^{-1}, but high levels were also measured on March 16, 2022 (Fig. 5D). In general, all variables were strongly influenced by the daily cycle, especially temperature, DO and Chl-*a* (Fig. 5).

The hydrographic profiler showed a vertical thermohaline gradient in the upper 20 m of the water column (Fig. 6A, B). Between January and February, surface temperatures remained above 16 °C, reaching maximum values >18 °C at the beginning of February (Fig. 6A). Thus, a double-layered water column structure was observed consisting of a warmer, fresher layer at the surface (estuarine water) and a colder and saltier layer below 20 m, caused by the inflow of a modified sub-Antarctic water mass. A pycnocline located at 5–10 m depth separated these two layers (Fig. 6B). High concentrations of DO persisted, with oversaturation conditions (>11.3 mg L^{-1} and 140 % saturation) occurring from December to February in the upper 20 m of the water column (Fig. 6C). The high thermohaline stratification conditions were accompanied by elevated concentrations of Chl-*a*, with maxima close to 50 μg L^{-1} at 8 m depth at the beginning of January 2022. At the beginning of March, the deep-water lower oxygen concentrations reached the surface, where a DO concentration of <8.4 mg L^{-1} and a saturation <90 % were recorded. Saturation decreased to 60 % at 35 m depth. In general, towards March and April, all variables decreased significantly (Fig. 6D). The decrease in oxygen saturation in March was concurrent with both the saltier and colder water column conditions and the slight increase in Chl-*a* near the surface (0–5 m; Fig. 6).

Dissolved inorganic nutrient (nitrate, nitrite and phosphate) concentrations were low in the surface layer (Fig. 6E–F) from December 2021 to April 2022, but the silicate concentration was low at the surface only between December and January. Maximum values of nitrates (28.3

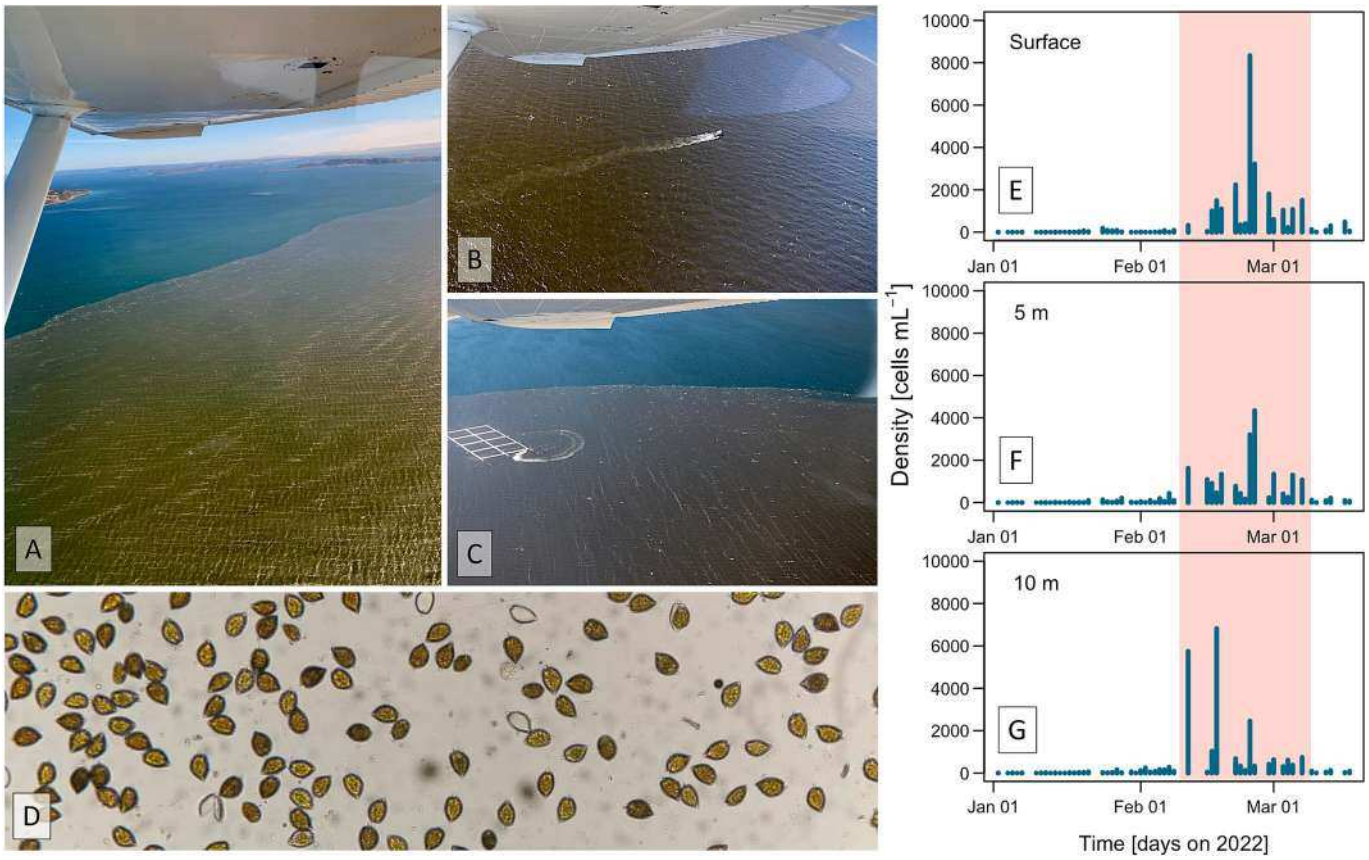

Fig. 4. A-D) Red tide caused by *Prorocentrum micans*. The photographs were taken at Reloncaví Sound and in the northern area of the Chiloe inland sea in February 2022. E-G) Daily variation of *P. micans* cell densities (data from the POAS Monitoring Program) at salmon farms located in Reloncaví Sound and northern Chiloé inland sea at the surface (upper left panel) and at depths of 5 m (middle left panel) and 10 m (lower left panel) from January 1 to March 24, 2022. Red shaded area corresponds to the cruise period.

μmol L^{-1}; Fig. 6E), phosphates (2.43 μmol L^{-1}; Fig. 6G) and silicates (26.9 μmol L^{-1}; Fig. 6H) were detected below 20 m, whereas nitrite values were highest (0.43 μmol L^{-1}) in an intermediate layer between 10 and 50 m (Fig. 6F). An injection of nutrient-rich water, mainly nitrate and silicate, from the bottom reached the surface layers (<20 m) on March 2022.

3.4. Oceanographic conditions during the *P. micans* bloom

CTD data from 18 sampling stations along the 420-km transect, from the head of Reloncaví Fjord to Corcovado Gulf, were spatially variable due to the coastal geomorphology of the region and the relative proximity to the Pacific Ocean (Fig. 7). The highest conservative surface temperature along the transect was 18 °C, measured at the photic layer (0–20 m depth) of the Reloncaví and Comau fjords (Fig. 7A) and occurring concomitantly with the presence of estuarine freshwater, an elevated buoyancy frequency (Brunt–Väisälä frequency, 120 cycles h^{-1}) and oxygen-oversaturated (120 %) water in the same layer (Fig. 7B–D). High values of pH (8.4–8.6) and Chl-*a* (~20 μg L^{-1}) were detected in the same areas and depths (Fig. 7E, F). Significant reductions in the temperature of the upper layer (0–20 m) occurred from the southern part of the Gulf of Ancud to the Gulf of Corcovado, coinciding with an increase in salinity (~33 g kg^{-1}).

Estuarine water (EW; 21–31 g kg^{-1}) was detected inside the two fjords (Reloncaví and Comau), a modified sub-Antarctic water mass (MSAAW; 31–33 g kg^{-1}) along the entire transect, and a sub-Antarctic water mass towards the south of the Gulf of Ancud (Fig. 7B).

The spatial distribution of *P. micans* cells in the upper layer of the water column (0–30 m depth) followed a pattern very similar to that of temperature, with the highest abundance occurring at the highest temperatures (Fig. 8). Thus, surface densities were highest in Reloncaví Sound and the Gulf of Ancud, with maximum values in the latter of >1 × 10^3 cells mL^{-1} (stations 7 and 12; Fig. 8A). South of the Desertores Islands, the cell density decreased significantly, with minimum values of 6 cells mL^{-1} measured at station 18, located in the Gulf of Corcovado.

Throughout the water column, the distribution of the cell density of *P. micans* was identical to that of Chl-*a*, suggesting the dominance of this species in the total phytoplankton community. Thus, at station 1, located at the head of Reloncaví Fjord and where a strong temperature (Δ 0-10 m; 2.1 °C) and haline (Δ 0-10 m; 18.6 g kg^{-1}) stratification was observed, maximum densities of 579 cells mL^{-1} occurred at 4 m depth whereas the densities at the surface and below 12 m depth did not exceed 4 cells mL^{-1} (Fig. 8B). At station 7 (Gulf of Ancud), densities >1.1 × 10^3 cells mL^{-1} were recorded at the surface but gradually decreased with depth, thus following the same pattern as Chl-*a*, which reached maximum values of 20 μg L^{-1} at the surface (Fig. 8C). At this station, the water column was vertically mixed. Finally, in the Gulf of Corcovado (station 18), where the water column was also mixed and with a lower temperature (12.2 °C), cell densities at the surface did not exceed 160 cells mL^{-1} and below 2 m they did not exceed 17 cells mL^{-1} (Fig. 8D).

The GLM-adjusted model for *P. micans* showed that salinity, dissolved oxygen, pH, and turbidity explained significantly ($p \leq 0.05$) a large fraction of the spatial variability of their cell abundance. No evidence of large effects of water temperature was found (Table 1; Fig. S2). However, according to the model β-coefficients, both salinity and pH conditions in the study area have a positive effect on cell abundance, but dissolved oxygen and turbidity impact it negatively (Table S1).

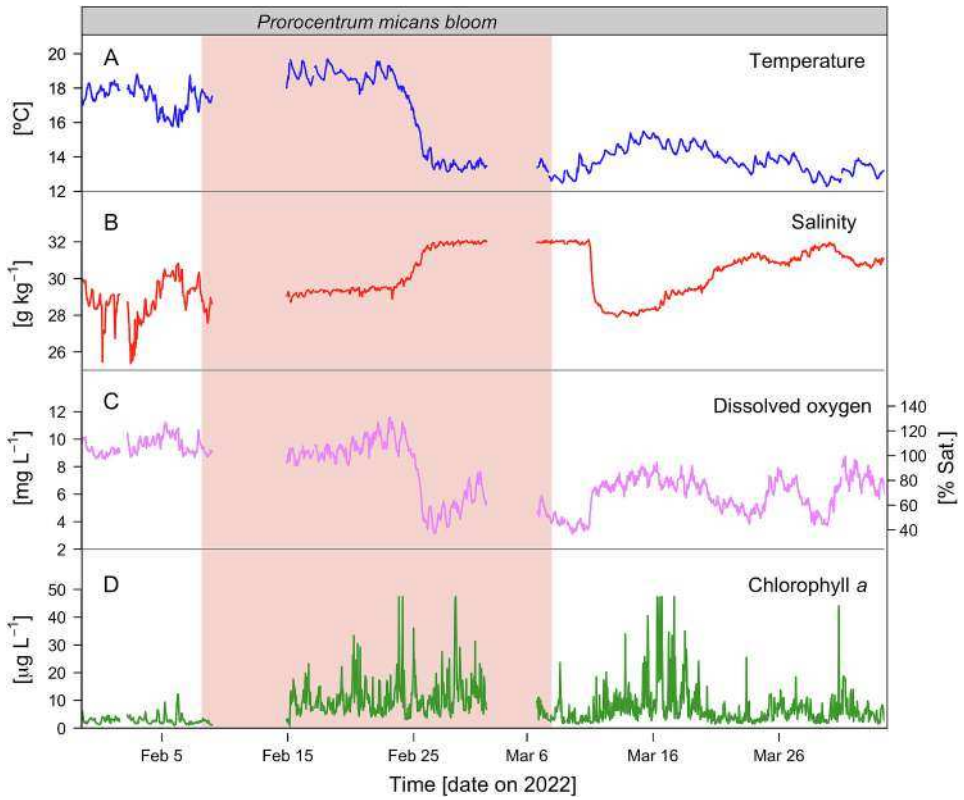

Fig. 5. Time series of A) SST (°C), B) salinity (g kg^{-1}), C) dissolved oxygen (mg L^{-1}) and D) chlorophyll *a*. The data were recorded hourly at the i ~ mar oceanographic buoy from February 1 to March 31, 2022.

3.5. Satellite images

Although images were downloaded for the period between February 10 and March 10, 2022, the only set that covered the entire study area and did not contain clouds was from February 22, 2022. The true-colour image showed an intense change in water colour, associated with the *P. micans* bloom, at the Gulf of Ancud and Reloncaví Sound (Fig. 9A). Both the Chl-*a* (Fig. 9B) and NDCI (Fig. 9C) images showed the patchy distribution of the *P. micans* bloom from the Desertores Islands to Puerto Montt. The highest Chl-*a* concentrations were detected in the Gulf of Ancud, suggesting it as an area of retention. In the Gulf of Corcovado, the colour change was associated with a discharge of riverine freshwater (e.g., from the Palena River). Within the Chiloé inland sea, the SST according to the GHRSST product was highest in Reloncaví Sound and the Gulf of Ancud, where the highest Chl-a and NDCI values were also recorded (Fig. 9D) coinciding with the area affected by the *P. micans* bloom. Nevertheless, this variable no shows a significance effect on *P. micans* cell density on GLM test (Table 1). High SST during February were also recorded during 2021 and 2023 (Fig. S3) and no blooms of *P. micans* were recorded in this area.

3.6. Modelling the surface circulation

The mean surface currents acquired through the MOSA model for the period spanning January to April 2022 revealed a southward-propagating current originating from the eastern side of Reloncaví Fjord (Fig. 10A). These currents tended to form cyclonic eddies centred in Reloncaví Sound and in the Gulf of Ancud (~ 73° W–42° S), coinciding with the highest SST, NDCI and Chl-*a* values (Fig. 10B–D). In January and the early weeks of February, the speed of this current remained at 0.4 m s^{-1}. Consequently, microalgae or floating objects were more prone to drifting and rotating within the eddy (Fig. 10B, C). The southward current gained strength starting from week 7 and reached its peak at week 9, when values exceeded 0.7 m s^{-1} (Fig. 10D, E). This current could have acted as a natural barrier for the renewal of water in Comau Fjord (42°13′ S; 72°30′ W). The simulated circulation patterns indicated enhanced retention in the area during January and early February, with a southward dispersion intensifying from mid-February onward, consistent with the decreases in temperature and radiation measured at the Comau Fjord weather station (data not show). From week 10, the southward current started to diminish, but the eddy persisted within the Ancud area (Fig. 10F, G).

3.7. Modelling particle tracking

The evolution of the *P. micans* bloom was approximated in two particle tracking experiments. In each one, 1000 surface particles were launched from the mouth of Reloncaví Fjord (Fig. 11). In the first experiment, the particles were released on February 8, 2022, just days before the detection of the bloom. In this scenario, the inert particles tended to circulate throughout Reloncaví Sound, covering it almost in its entirety over the course of the one-month experiment. The few particles that escaped via the southern boundary of Reloncaví Sound propagated in a near-direct southward pathway towards the Desertores Islands and Gulf of Corcovado (Fig. 11A). By contrast, in the second experiment, the particles released on February 23 accumulated in the southern part of Reloncaví Sound, exited at its southern boundary and dispersed into the Gulf of Ancud (Fig. 11B). Interestingly, the particles in this simulation followed much more erratic trajectories as they travelled towards the Desertores Islands, a behaviour that continued until the end of the simulation, on March 23.

4. Discussion

The interdisciplinary study conducted on the bloom led us to conclude that the high-biomass bloom of *P. micans* in NW Chilean

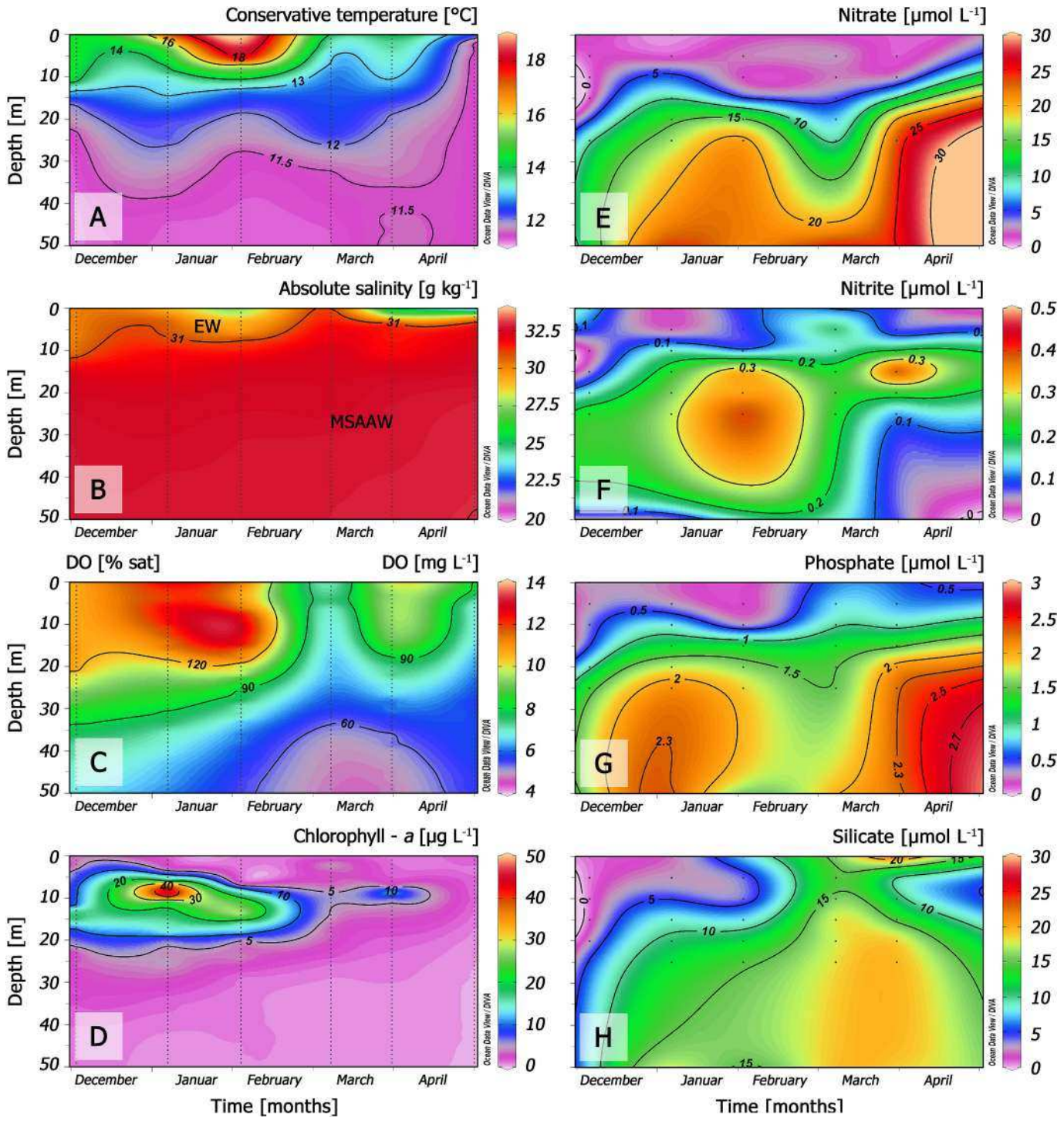

Fig. 6. Vertical distribution (0–50 m) of A) conservative temperature (°C), B) absolute salinity (g kg^{-1}), C) dissolved oxygen (mg L^{-1}), D) chlorophyll *a* (µg L^{-1}), E) nitrate (µM), F) nitrite (µM), G) phosphate (µM) and H) silicate (µM). The data were recorded monthly at the i ~ mar oceanographic buoy from December 2021 to April 2022.

Patagonia that developed in summer 2022 was the result of the interplay of local environmental drivers, as nutrient and current patterns, within a region subjected to increasing anthropogenic and climate change effects. Therefore, the presence of the bloom reflected a much larger context of changes, as the concurrent ocean and climatic conditions affecting coastal ecosystems have been shown to favour HB-HABs (Gobler, 2020; Wells et al., 2015).

4.1. Climate and anthropogenic modulations

Elevated cell densities of *P. micans* were first detected at shallow depths near the pycnocline in Reloncaví Sound, when the absolute temperature was high and salinity was low at the oxygenated surface layer. Concurrently, the near-surface water received nutrients from deeper waters, notably nitrites and silicates, which likely exacerbated the bloom. The bloom occurred when winds from the south and southeast were strongest, which could explain the replacement of the cold

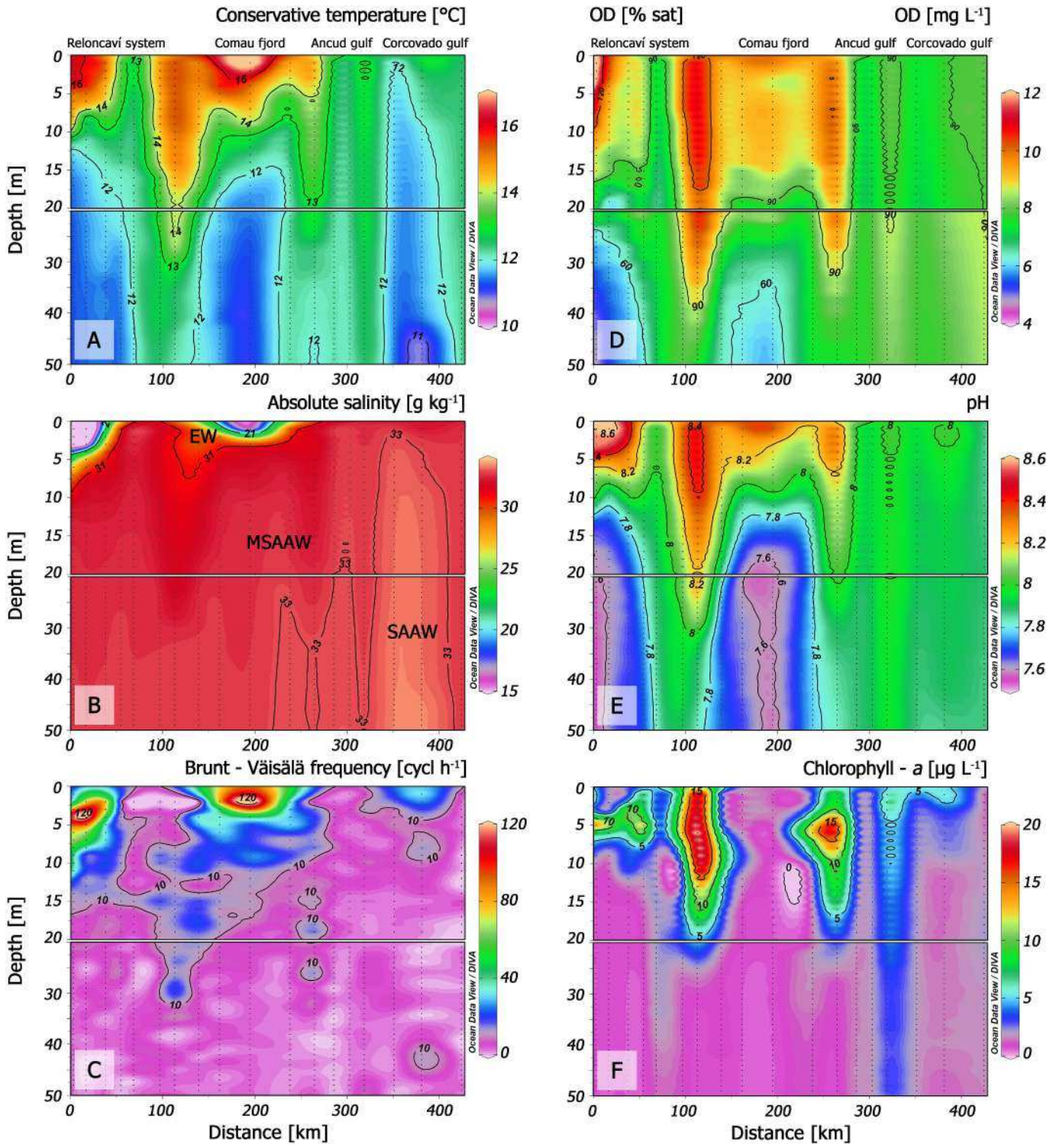

Fig. 7. Vertical distribution (0–50 m) of A) conservative temperature (°C), B) absolute salinity (g kg^{-1}), C) Brunt-Vaisälä frequency; D) dissolved oxygen (mg L^{-1}); E) pH and F) chlorophyll *a* (µg L^{-1}) measured at 18 sampling stations along a 420-km transect during a cruise from the head of Reloncaví Fjord to the Gulf of Corcovado from February 15 to March 4, 2022.

freshwater in the surface layer by warmer, saltier water at the time of the bloom. Satellite images combined with oceanic data showed that the distribution of the bloom was limited to areas of warmer temperatures and higher stratification influenced by coastal residual circulation patterns steered by the local geomorphology, which resulted in the production of vortical eddies able to accumulate or retain algal cells. Both the retention and the transport of HABs by eddies have been observed on the North American west coast (Anderson et al., 2006), in particular off the coast of Washington State (USA) (Trainer et al., 2002). The complex morphology of coastal areas, including headlands, islands and bathymetry gradients, has been shown to steer currents and produce eddy structures (Geyer and Signell, 1990; Zimmerman, 1978), which is likely also the case in the complex interconnected waterways of Northern Patagonia. *Prorocentrum micans* has been shown to form blooms

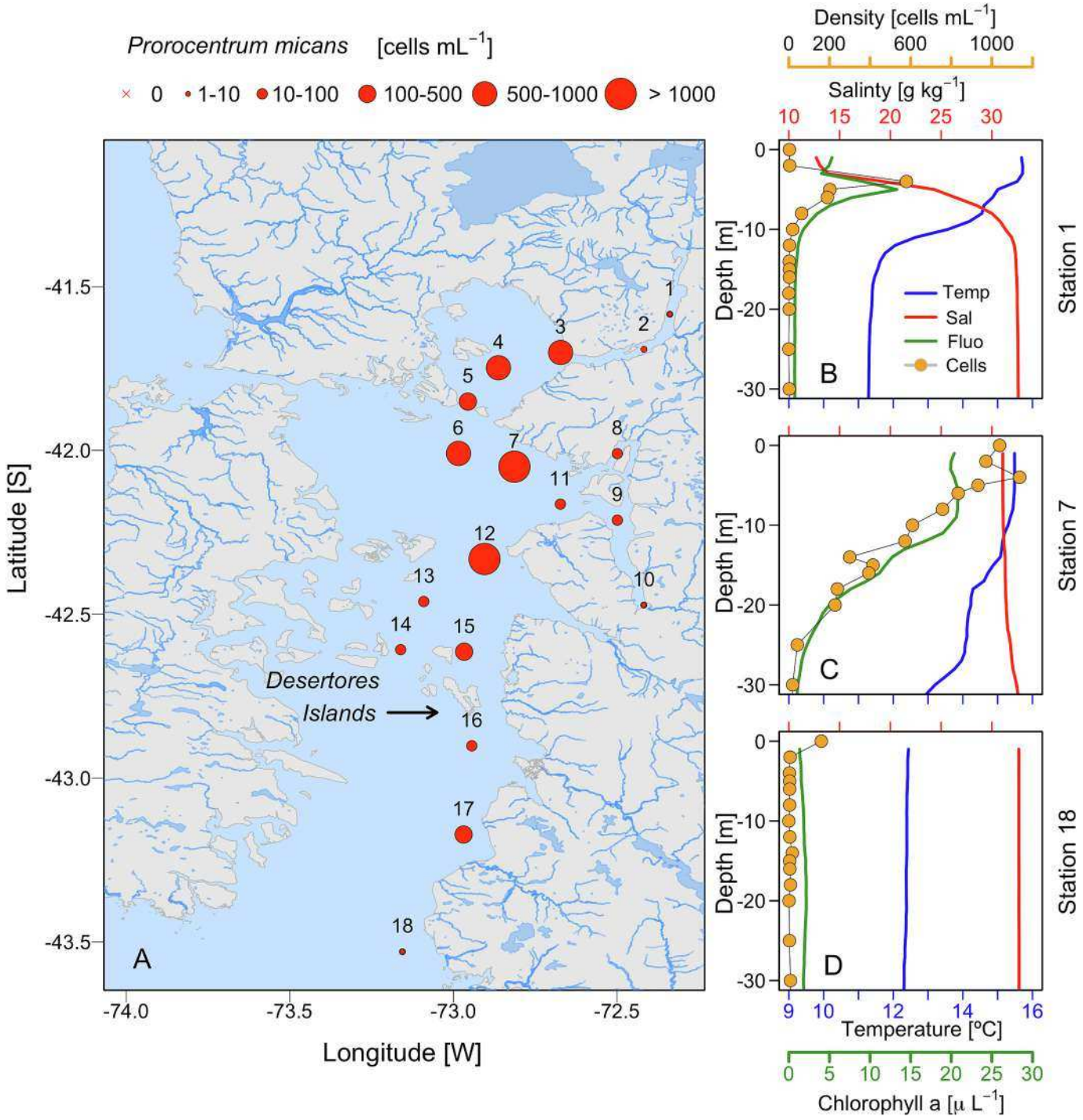

Fig. 8. A) Surface spatial distribution of *P. micans* cells at 18 sampling stations along a 420-km transect during a cruise from the head of Reloncaví Fjord to the Gulf of Corcovado from February 15 to March 4, 2022. Vertical distribution (0–30 m) of salinity (red line), temperature (blue line), chlorophyll *a* (green line) and *P. micans* cell densities at stations 1 (B), 7 (C) and 18 (D).

reaching high cell densities in several coastal areas around the globe, mainly in tropical and subtropical coastal areas, including those of tropical Japan (Fukuyo, 1981; Nishimura et al., 2020a; Nishimura et al., 2020b). In South America, *Prorocentrum* species were reported in Colombian Caribbean waters as early as 1977 (Arbeláez et al., 2017; Arbeláez et al., 2020; Loranzo-Duque et al., 2011; Mancena-Pineda et al., 2014; Rodríguez et al., 2010), and later in Brazil and Cuba (Arteaga-Sogamoso et al., 2023; Borasto et al., 2023; Moreira-González et al., 2019; Nascimento et al., 2016) and in Chile (Barría et al., 2022 and references therewithin). This global distribution reflects the affinity of *P. micans* for surface layers characterised by relatively high temperatures and higher salinities. Consequently, the air and water warming, increased stratification and altered solar radiation associated with climate change are altering the distribution, occurrence and blooming of this HAB species. Higher temperatures have been implicated in the steady increase in blooms of several toxic pelagic dinoflagellates, especially those thriving over a range of specific temperature niches (de Boer, 2005; Fehling et al., 2004; Li, 1980; Longhurst, 1998; Okolodkov, 2005; Rhodes and O'Kelly, 1994). Nonetheless, the temperatures that promote the proliferation of HAB dinoflagellates *in situ* are not those

Table 1
Statistical significance of explanatory variables determined using a X^2 test of marginal (type II) ANOVA for the variability of *P. micans* in the study area, using a Generalized Lineal Model (GLM) with logit link function for the residual negative binomial distribution.

Predictive variables	Chi square X^2	*df*	$Pr > (\|X^2\|)$
Temperature	0.364	1	0.546
Salinity	53.07	1	<0.001
Dissolved Oxygen	16.62	1	<0.001
pH	55.83	1	<0.001
Chlorophyll *a*	0.332	1	0.564
Tubidity	3.81	1	0.051

typically applied under laboratory conditions. Moreover, studies of *Prorocentrum* species (e.g., *P. lima* complex) have mainly focused on their abundance, distribution and toxicity whereas those examining their optimal growth in response to different environmental factors, notably temperature, are scarce (Hashimoto et al., 2021). The optimal growth of *P. micans*, the type species of the genus, has been investigated only recently, in the context of a future high temperature and high radiation scenario. The authors reported the inhibition of *P. micans* growth under high temperature but its promotion under high light exposure, through the upregulation of photosynthesis, antioxidase activity, protein folding, and degradation of proteins (Zhang et al., 2022). For *P. lima*, temperature was shown to outweigh the effects of salinity, photoperiod and light intensity on its growth (Grigoryan et al., 2024). However, in natural systems, growth is the result of multiple factors that together produce optimal conditions (Karentz and Smayda, 1984; Karentz and Smayda, 1998).

Nonetheless, the effects of warming on HB-HAB occurrence shows a trend of an expansion into higher latitudes, making Chilean Patagonia particularly vulnerable to these blooms in the future (Wells et al., 2015). The stratification associated with warming, glacial and snow melting, and precipitation runoff at high latitudes has been shown to increase the occurrence of toxic pelagic dinoflagellates, but whether its effect on HB-HABs is positive or negative is unknown. However, the same local drivers (the interplay of wind effects, irradiance, hydrography, the depth and intensity of the pycnocline, runoff, and nutrients) related to causative agents of unusually intense toxic blooms (Wells et al., 2015 and references therewithin) were the same as those that resulted in the exceptional HB-HAB of *P. micans* in the study area in summer 2022.

Climate change and current patterns are not the sole effectors and predictors of HABs in coastal waters. Rather, eutrophication has been changing the occurrence of HABs in coastal ecosystems and is an additional stressor in systems affected by warming, acidification, and deoxygenation (Gobler, 2020; Griffith and Gobler, 2020). Nutrients, notably N, P and Si, govern primary production and the succession of HAB species within plankton communities. High-biomass blooms of pelagic *Prorocentrum* species, associated with the disruption of food webs, have typically been recorded in nearshore coastal areas enriched in N and P (Heil et al., 2005). Those same conditions played a role in the occurrence of *P. micans* in Chilean Patagonia in summer 2022. Increased levels of subsurface nutrients, including lithogenic and biogenic Si of riverine origin and following a north-south gradient along the Chilean coast, are well documented (Chase et al., 2014; Sánchez et al., 2008; Sarmiento et al., 2004). Of particular interest for *P. micans* HB-HABs is the increased loads of N and P in coastal areas, attributable to the dramatic increase in human activities since 2015 that has shifted nutrient availability for HAB species, including the expansion of land transformation, agriculture and aquaculture (Beussen et al., 2022; Glibert et al., 2008). In Chilean Patagonia, this shift is associated with the development of salmon aquaculture, the change in freshwater runoff induced by the climate-change-driven increases in drought and melting ice as well as nutrient enrichment from agriculture, tourism and industry, all of which threaten the integrity of marine ecosystems, notably those at the marine-terrestrial interface (Buschmann et al., 2023; Rozzi et al., 2023). In particular, N enrichment of coastal ecosystems has changed the N:P ratios and the stoichiometry of these major nutrients, although the consequences for HAB species have yet to be studied (Glibert, 2017). According to an oceanographic-biogeochemical model in which the parametrisation included changes in nutrient forms and ratios due to ocean warming, *Prorocentrum* spp. blooms will likely expand into Northeast Europe/Baltic Sea and Northeast Asia (Glibert et al., 2014). The effects of this expansion will be particularly significant

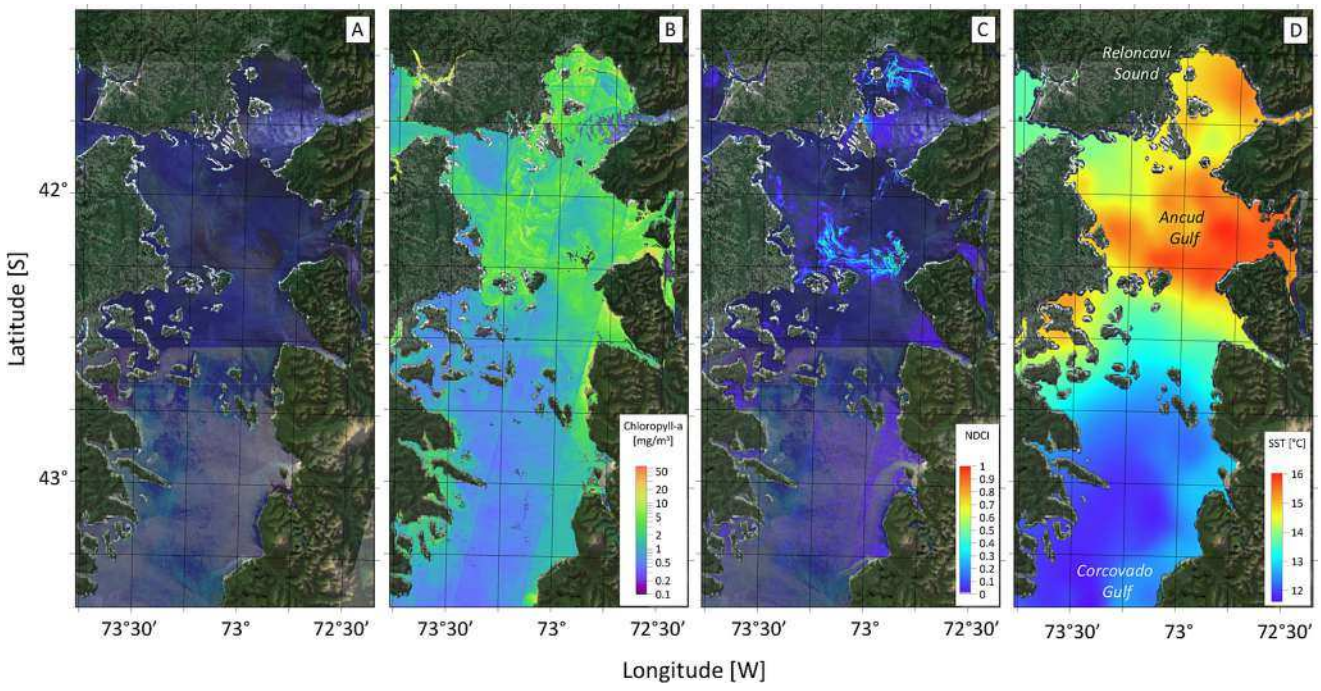

Fig. 9. High-resolution (10 m) Sentinel-2 images of A) true colour, B) chlorophyll *a* (μg L^{-1}); C) normalized difference chlorophyll index (NDCI) and D) SST from the product of level 4 GHRSST along the Chiloé inland sea, from Reloncaví Sound to the Gulf of Corcovado, on February 22, 2022.

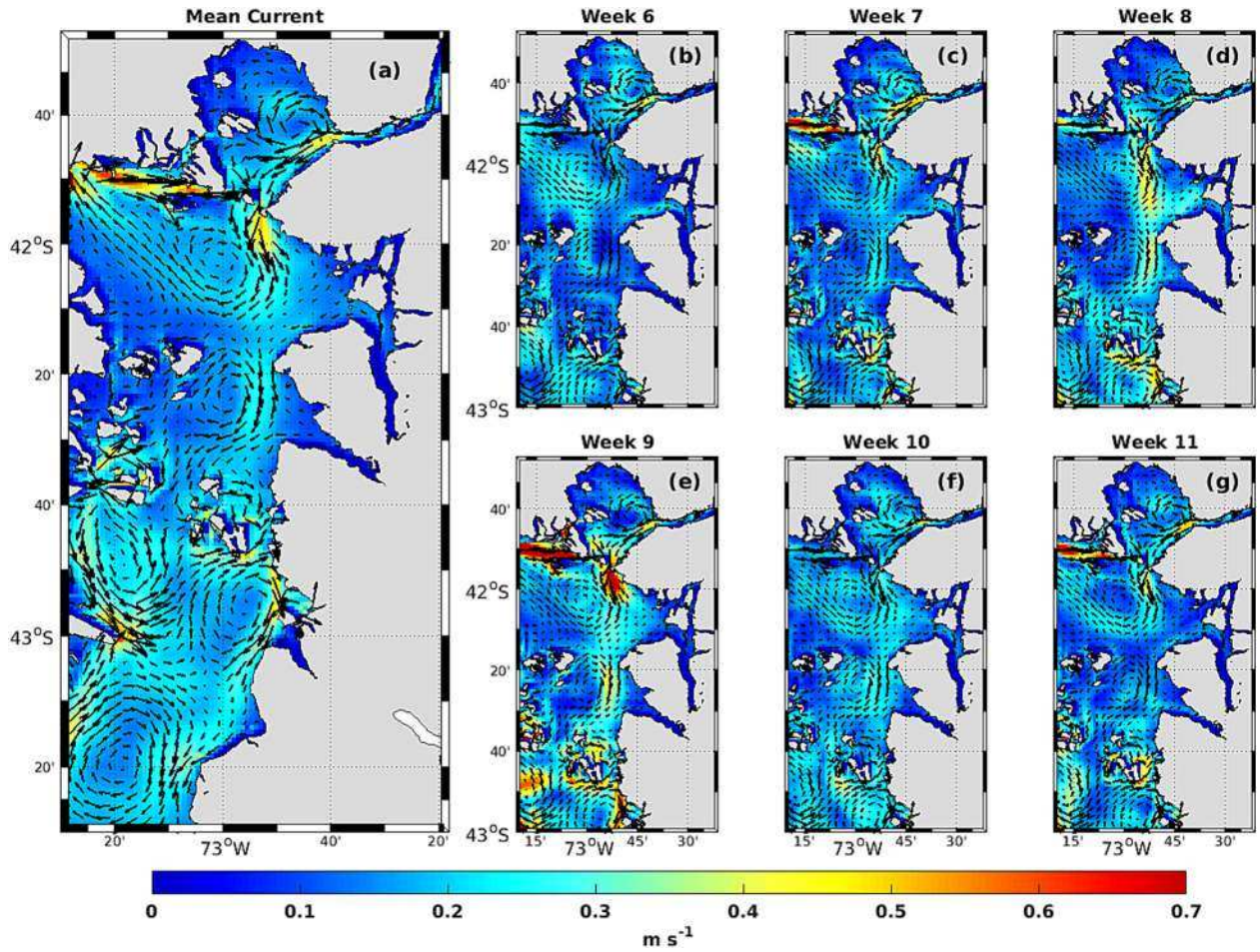

Fig. 10. A) Average surface current in the Inner Sea of Chiloé from January to April 2022 obtained from the MOSA operational model, and B-G) average weekly surface current. Week 6 corresponds to the second week of February, and week 11 corresponds to the third week of March.

in Asia, where aquaculture is a major economic activity and agricultural N-based fertilizers are replacing P-based fertilizers, resulting in even higher N:P ratios and the further expansion of *Prorocentrum* spp. HABs (Bouwman et al., 2009; Bouwman et al., 2013; Bouwman et al., 2011; Cordell et al., 2009; Glibert et al., 2012; Glibert et al., 2008; Glibert et al., 2005b). Similarly, the high-biomass bloom of *P. micans* in Chilean Patagonia in summer 2022 can be attributed to climate-induced warming and stratification coupled with high N loads from the salmon aquaculture, agricultural and land-based industries and their associated activities (Glibert, 2020; Marquet et al., 2023; Wells et al., 2020).

4.2. Transport and retention mechanisms of HB-HAB

Coastal circulation has been found to be a key factor in the transport and abundance of HABs (Glibert et al., 2005a; Pitcher et al., 2010; Quin and Shen, 2019). Complex coastal geomorphological features, such as islands, headlands, and changes in bathymetry, can influence coastal circulation patterns by redirecting tidal flows and generating localized rotation (vorticity) in the water (Geyer and Signell, 1990; Pingree, 1978; Signell and Geyer, 1991; Zimmerman, 1978). This vorticity can lead to the formation of eddies, which may occur during specific tidal phases (Brooks et al., 1999; Signell and Geyer, 1991), specific weather conditions (Li and Weeks, 2009) or persist in residual flows as "residual eddies" (Bailey et al., 2024; Robinson, 1981; Zimmerman, 1978; Zimmerman, 1981). These eddies can influence water exchange between estuaries and the open ocean (e.g., Yang and Wang, 2013), thus affecting the transport, accumulation and retention of material in coastal areas. Understanding such dynamics are particularly relevant for aquaculture management during HAB events.

Previous studies have linked eddies to the retention and movement of HABs (Anderson et al., 2006). Others have shown that eddies can exacerbate HABs by limiting phytoplankton dispersal or enhancing growth by bringing essential nutrients to the surface (Coria-Monter et al., 2017). In a recent study, Bailey et al. (2024) demonstrated that residual eddies created algal cell accumulation hotspots in a geomorphologically complex deglaciated coastal area in the northeast United States. The findings of this study align with their results, showing that the complex coastline and bathymetry of Northern Patagonia also generate vortical eddies in the mean current velocities. For example, an eddy that persistently appears in the mean flow of the Gulf of Ancud (Fig. 10) could serve as a hotspot for the accumulation of HAB or HB-HAB cells. Satellite images of Chl-a and NDCI (Fig. 9B-C) further support this, revealing elevated values of these parameters along the periphery of the eddy in the gulf. Additionally, the elevated counts of *P. micans* cells in the Gulf of Ancud, near the periphery of the eddy, confirm the presence of a material accumulation hotspot for HABs and HB-HABs.

4.3. Future perspectives under the Patagonia climate scenario

Both HABs and HB-HABs will likely increase at high latitudes, driven by local and regional environmental drivers, including climate change stressors as well as anthropogenic activities on land, at the land-water interface and in coastal areas. Under future climate scenarios and increased anthropogenically driven nutrient loading, the range of HB-HABs of *Prorocentrum* can be expected to expand, encompassing NW

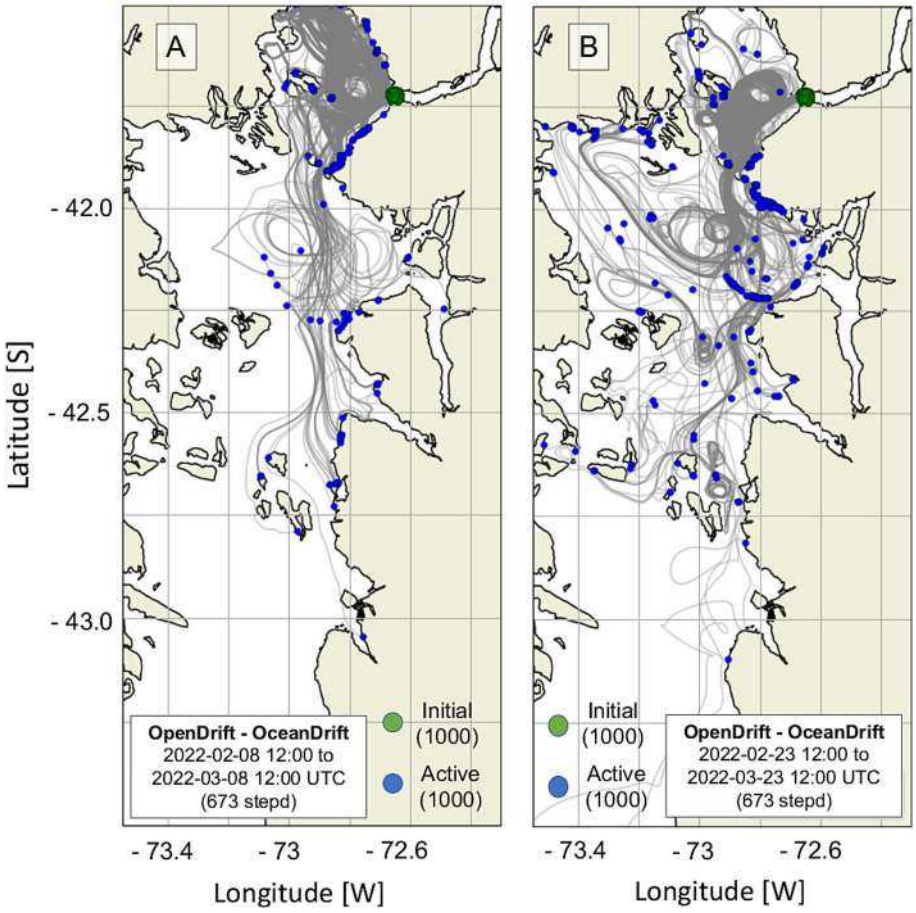

Fig. 11. Particle tracking experiments to approximate the evolution of the *Prorocentrum micans* bloom using the Opendrift Model. A) Trajectories of 1000 particles over a 1-month simulation released on February 8 (2 days before the bloom started). B) Trajectories of 1000 particles over a 1-month simulation released on February 23 (during the peak of cell density). Initial denote the position of the particles were released, while active shows the final position after 30-day particle experiment.

Europe and Northern Asia. South America is subjected to several stressors that affect both its land and coastal ecosystems. In Chilean Patagonia, higher temperatures, radiation levels and nutrient loads together with reduced precipitation have already increased HAB events, a major ocean stressor that has caused mass mortalities of fish. Marine resources are also particularly vulnerable to ocean warming and increasing ENSO extreme events coupled with ocean acidification and deoxygenation. A high-biomass bloom of *P. micans* in NW Patagonia, comparable to that in summer 2022, could therefore develop, as climate change, aquaculture and land-based anthropogenic activities continue to exert pressure on coastal ecosystems. Chilean Patagonia provides a natural laboratory for studies of the responses of HB-HAB such as *P. micans*, including how these food-web-disruptive algae respond to climate change and eutrophication at high latitudes. The knowledge gained in those studies will support the improved management of the unique ecosystems and biodiversity of the region and reduce the socio-economic impacts of HABs (Marquet et al., 2023).

Finally, in the context of evaluating the factors surrounding a future scenario of HB-HABs of *P. micans* in this area, we cannot forget to include other potential associated negative side-effects for human activities. For example, communities in several districts of Puerto Montt, a port city located at the northern end of Reloncaví Sound, reported a strong smell of sulfuric gas on March 3, 2022, coinciding with final the phase of the *P. micans* bloom. Given that *P. micans* produced DMS at relatively low densities, as shown by lab-based experiments and in the field (Cyronak et al., 2014; Li et al., 2021), the pungent ("rotten egg") smell reported in Los Lagos during the bloom of *P. micans* could be have originated from the bloom itself.

5. Conclusions

In late summer of 2022, a high-biomass bloom of the non-toxic dinoflagellate *Prorocentrum micans* occurred in northwest Chilean Patagonia. Although local hydrographic conditions were in part responsible for the formation and maintenance of the bloom, the latitudinal expansion recorded for this species blooms suggests that climate change related conditions can be favouring its formation, particularly higher irradiance, water temperature and salinity. HB-HABs are in general less studied than those blooms caused by toxic species. However, they can greatly impact the economy of coastal areas, because low oxygen environments associated to this HB-HABs can cause mass fish mortalities, being aquaculture being a key industry in Chile. Additionally, more research is needed in order to evaluate the potential health impact that could be generated from the capacity of this species to produce Dimethyl sulfide (DMS), which has been reported to cause irritation of eyes and skin, and even affect the central nervous system.

CRediT authorship contribution statement

Patricio A. Díaz: Writing – review & editing, Writing – original draft, Visualization, Software, Resources, Project administration, Methodology, Investigation, Funding acquisition, Formal analysis, Data curation, Conceptualization. **Leila Basti:** Writing – review & editing, Writing – original draft, Validation, Methodology, Investigation, Formal analysis, Conceptualization. **Iván Pérez-Santos:** Writing – review & editing, Writing – original draft, Resources, Project administration, Methodology, Investigation, Funding acquisition, Formal analysis,

Conceptualization. **Camila Schwerter:** Writing – review & editing, Writing – original draft, Visualization, Software, Methodology, Investigation, Formal analysis. **Osvaldo Artal:** Writing – review & editing, Writing – original draft, Visualization, Validation, Software, Resources, Methodology, Formal analysis, Conceptualization. **Sergio A. Rosales:** Writing – review & editing, Writing – original draft, Visualization, Validation, Software, Methodology, Formal analysis. **Lauren Ross:** Writing – review & editing, Writing – original draft, Validation, Formal analysis. **René Garreaud:** Writing – review & editing, Writing – original draft, Visualization, Validation, Software, Resources, Methodology, Investigation, Formal analysis, Conceptualization. **Carlos Conca:** Writing – review & editing, Writing – original draft, Supervision, Resources. **Gonzalo Álvarez:** Writing – review & editing, Writing – original draft, Visualization, Validation, Methodology, Investigation, Formal analysis, Conceptualization. **Zoë L. Fleming:** Writing – review & editing, Writing – original draft, Validation, Formal analysis. **Fabiola Villanueva:** Writing – review & editing, Formal analysis, Data curation. **Manuel Díaz:** Writing – review & editing, Visualization, Software, Investigation, Formal analysis. **Guido Mancilla-Gutiérrez:** Writing – review & editing, Visualization, Methodology, Investigation. **Robinson Altamirano:** Writing – review & editing, Visualization, Methodology, Investigation. **Camilo Rodríguez-Villegas:** Writing – review & editing, Visualization, Methodology, Investigation. **Pamela Urrutia:** Writing – review & editing, Formal analysis, Data curation. **Geysi Urrutia:** Writing – review & editing, Formal analysis, Data curation. **Pamela Linford:** Visualization, Software, Investigation, Formal analysis. **Tomás Acuña-Ruz:** Visualization, Software, Investigation, Formal analysis. **Rosa I. Figueroa:** Writing – review & editing, Writing – original draft, Visualization, Supervision, Resources, Methodology, Investigation, Conceptualization.

Declaration of competing interest

We have not financial interests/personal relationships which may be considered as potential competing interests.

Acknowledgements

This work was supported by project RTI10-22, funded by Vicerrectoría de Investigación y Postgrado, Universidad de Los Lagos. Patricio A. Díaz was funded by the ANID-FONDECYT 1231220 and by the Centre for Biotechnology and Bioengineering (CeBiB) (PIA project AFB240001, ANID, Chile), both from the Chilean National Agency for Research and Development (ANID). Iván Pérez-Santos was funded by COPAS COASTAL (ANID FB210021), CIEP R20F002, and FONDECYT 1211037. Osvaldo Artal was partially funded by COPAS Coastal ANID FB210021. Lauren Ross received a Fulbright U.S. Scholar grant during the research that led to this publication. Carlos Conca was partially supported by CMM FB210005 & CeBiB AFB240001 projects. Pamela Linford was funded by COPAS Coastal ANID FB210021. Rosa I. Figueroa was funded by a grant for Galician Networks of Excellence (GPC-VGO-HAB (IN607B 2023/11) from the Innovation Agency of the Xunta de Galicia (GAIN) and BIOTOX (PID2021-125643OB-C22), AEI, Spanish Ministry of Science, Innovation and Universities. This is a contribution to SCOR WG #165 MixONET which is supported by grant OCE-214035 from the National Science Foundation to the Scientific Committee on Oceanic Research (SCOR) and contributions from SCOR National Committees.

Appendix A. Supplementary data

Supplementary data to this article can be found online at https://doi.org/10.1016/j.scitotenv.2024.178140.

Data availability

Data will be made available on request.

References

Akaike, H., 1974. A new look at the statistical model identification. IEEE Trans Automat Contr 19, 716–723.
Álvarez, G., Uribe, E., Díaz, R., Braun, M., Mariño, C., Blanco, J., 2011. Bloom of the yessotoxin producing dinoflagellate *Protoceratium reticulatum* (Dinophyceae) in northern Chile. J. Sea Res. 65, 427–434.
Álvarez-Garreton, C., Mendoza, P.A., Boisier, J.P., Addor, N., Galleguillos, M., Zambrano-Bigiarini, M., et al., 2018. The CAMELS-CL dataset: catchment attributes and meteorology for large sample studies – Chile dataset. Hydrol. Earth Syst. Sci. 22.
Anderson, C.R., Brzezinski, M.A., Washburn, L., Kudela, R., 2006. Circulation and environmental conditions during a toxigenic *Pseudo-nitzschia australis* bloom in the Santa Barbara Channel, California. Mar. Ecol. Prog. Ser. 327, 119–133.
Arbeláez, N., Mancera, J.E., Reguera, B., 2017. Epiphytic dinoflagellates of *Thallasia testudinium* two coastal systems of the Colombian Caribbean. Boletín de Investigaciones Marinas y Costeras 46, 9–40.
Arbeláez, N., Mancera, J.E., Reguera, B., 2020. Structural variation of potentially toic epiphytic dinoflagellates on *Thallasia testudinium* from two coastal systems of the Colombian Caribbean. Harmful Algae 92, 101738.
Arteaga-Sogamoso, E., Rodríguez, F., Amato, A., Ben-Gigirey, B., Fraga, S., Mafra Jr., L. L., et al., 2023. Morphology and phylogeny of *Prorcentrum porosum* sp. Nov. (Dinophyceae): a new benthic toxic dinoflagellate from the Atlantic and Pacific Oceans. Harmful Algae 121, 102356.
Bailey, T., Ross, L., Tiner, N., Smith, S.M.C., Perez-Santos, I., Ramos, A., et al., 2024. Geomorphological controls on estuary hydrodynamics with implications for diatom blooms in deglaciated coastal areas. Sci. Total Environ. 948, 174902.
Baldrich, A.M., Díaz, P.A., Rosales, S.A., Rodríguez-Villegas, C., Álvarez, G., Pérez-Santos, I., et al., 2024. An unprecedented bloom of oceanic dinoflagellates (*Karenia* spp.) inside a fjord within a highly dynamic multifrontal ecosystem in Chilean Patagonia. Toxins 16, 77.
Barría, C., Vasquez-Calderon, P., Lizama, C., Herrera, P., Canto, A., Conejeros, P., et al., 2022. Spatial temporal expansión of harmful algal blooms in Chile: a review. J. Mar. Sci. Eng. 10, 1868.
Bedriñana-Romano, L., Viddi, F.A., Artal, O., Pinilla, E., Hucke-Gaete, R., 2023. First estimate of distribution, abundance, and risk of encounter with aquaculture vessels for the rare Chilean dolphin in the entire Northern Chilean Patagonia. Aquat. Conserv. Mar. Freshwat. Ecosyst. 33, 1535–1551.
Beggs, H., Karagali, I., Castro, S., 2023. Sea surface temperature: an introduction to users on the set of GHRSST formatted products (1/2023). Zenodo. https://doi.org/10.5281/zenodo.7589540.
Beussen, A.H.W., Doelman, J.C., Van Beek, L.P.H., Van Puijenbroek, P.J.T.M., Mogollón, J.M., Van Grinsven, H.J.M., et al., 2022. Exploring river nitrogen and phosphorus loading and export to global coastal waters in the Shared Socio-economic pathways. Glob. Environ. Chang. 72, 102426.
Boisier, J.P., Alvarez-Garreton, C., Cordero, R., Damian, A., Gallardo, L., Garreaud, R., et al., 2019. Anthropogenic drying in central-southern Chile evidenced by long term observations and climate model simulations. Elementa Sci. Anthropocene 6, 74.
Borasto, G.T., Salgueiro, F., GAL, De'Carli, Morais, A.M., Goulart, A.S., de Paula, J.C., et al., 2023. Taonomy and abundance of epibenthic *Prorocentrum* (Dinophyceae) species from the tropical and subtropical Southwest Atlantic Ocean including a review of their global diversity and distribution. Harmful Algae 127, 102470.
Bouwman, A.F., Beusen, A.H.W., Billen, G., 2009. Human alteration of the global nitrogen and phosphorus soil balances for the period 1970–2050. Global Biogeochem. Cycles 23, GB0A04.
Bouwman, A.F., Pawlowski, M., Liu, C., Beusen, A.H.W., Shumway, S.E., Glibert, P.M., et al., 2011. Global hindcasts and future projections of coastal nitrogen and phosphorus loads due to shellfish and seaweed aquaculture. Rev. Fish. Sci. 19, 331–357.
Bouwman, A.F., Beusen, A.H.W., Overbeek, C.C., Bureau, D.P., Pawlowski, M., Glibert, P. M., 2013. Hindcasts and future projects of global inland and coastal nitrogen and phosphorus loads due to finfish aquaculture. Rev. Fish. Sci. 21, 112–156.
Brooks, D.A., Baca, M.W., Lo, Y.T., 1999. Tidal circulation and residence time in a macrotidal estuary: Cobscook Bay, Maine. Estuar. Coast. Shelf Sci. 49, 647–665.
Buschmann, A.H., Niklitschek, E.J., Pereda, S.V., 2023. Aquaculture and its impacts on the conservation of Chilean Patagonia. In: Castilla, J.C., Armesto, J.J., Martínez-Harms, M.J., Tecklin, D. (Eds.), Conservation in Chilean Patagonia: Assessing the State of Knowledge, Opportunities, and Challenges. Springer Nature Switzerland AG, pp. 303–320.
Cabello, F.C., Godfrey, H.P., 2016. Harmful algal blooms (HABs), marine ecosystems and human health in the Chilean Patagonia. Rev. Chilena Infectol. 33, 559–560.
Chase, Z., McManus, J., Mix, A.C., Muratli, J., 2014. Southern-ocean and glaciogenic nutrients control diatom export production on the Chile margin. Quat. Sci. Rev. 99, 135–145.
Cordell, D., Drangert, J.-O., White, S., 2009. The story of phosphorous: global food security and food for thought. Glob. Environ. Chang. 19, 292–305.
Coria-Monter, E., Monreal-Gómez, M.A., Salas de León, D.A., Merino- Ibarra, M., Durán-Campos, E., 2017. Wind driven nutrient and subsurface chlorophyll-a enhancement in the Bay of La Paz, Gulf of California. Estuar. Coast. Shelf Sci. 196, 290–300.

Cyronak, T., O'Reilly, E., Lee, P.A., DiTullio, G.R., 2014. *In situ* determination of celular DMSP and pigment quotas in *Prorocentrum minimum* bloom near Flakland Islands. Adv. Oceanogr. Limnol. 2, 123–140.
Dagestad, K.-F., Röhrs, J., Breivik, O., Adlandsvik, B., 2018. OpenDrift v1.0: a generic framework for trajectory modelling. Geosci. Model Dev. 11, 1405–1420.
de Boer, M.K., 2005. Temperature responses of three *Fibrocapsa japonica* strains (Raphidophyceae) from different climate regions. J. Plankton Res. 27, 47–60.
Debreu, L., Marchesiello, P., Penven, P., Cambon, G., 2012. Two-way nesting in split-explicit ocean models: algorithms, implementation and validation. Ocean Model. 49, 1–21.
Díaz, P.A., Figueroa, R.I., 2023. Toxic algal bloom recurrence in the era of global change: lessons from the Chilean Patagonian fjords. Microorganisms 11, 1874.
Díaz, P.A., Álvarez, A., Varela, D., Pérez-Santos, I., Díaz, M., Molinet, C., et al., 2019. Impacts of harmful algal blooms on the aquaculture industry: Chile as a case study. Perspect. Phycol. 6, 39–50.
Díaz, P.A., Pérez-Santos, I., Álvarez, G., Garreaud, R., Pinilla, E., Díaz, M., et al., 2021. Multiscale physical background to an exceptional harmful algal bloom of *Dinophysis acuta* in a fjord system. Sci. Total Environ. 773, 145621.
Díaz, P.A., Álvarez, G., Pizarro, G., Blanco, J., Reguera, B., 2022. Lipophilic toxins in Chile: history, producers and impacts. Mar. Drugs 20, 122.
Díaz, P.A., Pérez-Santos, I., Basti, L., Garreaud, R., Pinilla, E., Barrera, F., et al., 2023. The impact of local and climate change drivers on the formation, dynamics, and potential recurrence of a massive fish-killing microalgal bloom in Patagonian fjord. Sci. Total Environ. 865, 161288.
Díaz, P.A., Álvarez, G., Schwerter, C., Baldrich, A., Pérez-Santos, I., Díaz, M., et al., 2024a. Synchronic distribution of the dinoflagellate *Protoceratium reticulatum* and yessotoxins in a high stratified fjord system: tidal or light modulation? Harmful Algae 135, 102649.
Díaz, P.A., Araya, M., Cantarero, B., Miranda, C., Varela, D., Figueroa, R.I., et al., 2024b. Are yessotoxins an emerging problem in Chile? Context and perspectives following the first report of YTX levels exceeding the regulatory limit in the Patagonian fjord system. Environ. Pollut. 361, 124844.
Dumont, E., Harrison, J.A., Kroeze, C., Bakker, E.J., Seitzinger, S.P., 2005. Global distribution and sources of dissolved inorganic nitrogen export to the coastal zone: results from a spatially explicit, global model. Global Biogeochem. Cycles 19, GB4S02.
Ehrenberg, C.G., 1834. Dritter Beitrag zur Erkenntniss grosser Organisation in der Richtung des kleinsten Raumes. Abhandlungen der Königlichen Akademie der Wissenschaften zu Berlin 1833, 145–336 pls I-XIII.
Fehling, J., Green, D., Davidson, K., Bolch, C., Bates, S., 2004. Domoic acid production by *Pseudo-nitzschia seriata* (Bacillarophyceae) in Scottish Waters. J. Phycol. 40, 622–630.
Fogt, R.L., Marshall, G.J., 2020. The southern annular mode: variability, trends, and climate impacts across the southern hemisphere. WIREs Clim. Chang. 11, e652.
Fox, J., Weisberg, S., 2011. An R Companion to Applied Regression. Sage, Thousand Oaks.
Fukuyo, Y., 1981. Taxonomical study on benthic dinoflagellates collected in coral reefs. Bull. Jpn. Soc. Sci. Fish. 47, 967–978.
Garreaud, R., 2018. Record-breaking climate anomalies lead to severe drought and environmental disruption in western Patagonia in 2016. Climate Res. 74, 217–229.
Geyer, W.R., Signell, R., 1990. Measurements of tidal flow around a headland with a shipboard acoustic Doppler current profiler. J. Geophys. Res. Oceans 95, 3189–3197.
Glibert, P.M., 2017. Eutrophication, harmful algae and biodiversity – challenging paradigms in a world of complex nutrient changes. Mar. Pollut. Bull. 124, 591–606.
Glibert, P.A., 2020. Harmful algae at the complex nexus of eutrophication and climate change. Harmful Algae 91, 101583.
Glibert, P.M., Anderson, D.M., Gentien, P., Granelí, E., Sellner, K.G., 2005a. The global and complex phenomena of harmful algal blooms. Oceanography 18, 136–147.
Glibert, P.M., Seitzinger, S., Heil, C.A., Burkholder, J.M., Parrow, M.W., Codispoti, L.A., et al., 2005b. The role of eutrophication in the global proliferation of harmful algal blooms: new perspectives and new approaches. Oceanography 18, 198–209.
Glibert, P.M., Mayorga, E., Seitzinger, S., 2008. *Prorocentrum minimum* tracks anthropogenic nitrogen and phosphorus inputs on a global basis: application of spatially explicit nutrient export models. Harmful Algae 8, 33–38.
Glibert, P.M., Burkholder, J.M., Kana, T.M., 2012. Recent insights about relationships between nutrient availability, forms, and stoichiometry, and the distribution, ecophysiology, and food web effects of pelagic and benthic *Prorocentrum* species. Harmful Algae 14, 231–259.
Glibert, P.M., Allen, J.I., Artioli, Y., Beusen, A., Bouwman, L., Harle, J., et al., 2014. Vulnerability of coastal ecosystems to changes in harmful algal blooms distribution in response e to climate change: projections based on model analysis. Glob. Chang. Biol. 20, 3845–3858.
Gobler, J.C., 2020. Climate change and harmful algal blooms: Insignts and perspective. Harmful Algae 91, 101731.
Gómez, F., 2005. A list of free-living dinoflagellate species in the world's oceans. Acta Bot. Croata 64, 129–212.
Grasshoff, K., Ehrhardt, M., Kremling, K., 1983. Methods of Seawater Analysis. Vol 2nd Edition. Verlag Chemie Weinhein, New York, USA.
Griffith, A.W., Gobler, C.J., 2020. Harmful algal blooms: a climate change co-stressor in marine and freshwater ecosystems. Harmful Algae 91, 101590.
Grigoryan, A., Lorini, M.L., Figueiredo, MdSL, Almada, E.V.C., Nascimento, S.M., 2024. Effects of culture conditions on the growth of the benthic dinoflagellates *Ostreopsis* cf. *ovata*, *Prorocentrum lima* and *Coolia malayensis* (Dinophyceae): a global review. Harmful Algae 132, 102565l.
Grzebyk, D., Denardou, A., Berland, B., Pouchus, Y.F., 1997. Evidence of a new toxin in the redtide dinoflagellate *Prororcentrum minimum*. J. Plankton Res. 19, 1111–1124.
Harrison, J.H., Caraco, N.F., Seitzinger, S.P., 2005. Global patterns and sources of disolved organic matter export to the coastal zone: results from a spatially explicit, global model. Global Biogeochem. Cycles 19, GB4S04.
Harrisson, J.H., Seitzinger, S.P., Caraco, N., Bouwman, A.F., Beusen, A., Vörösmarty, C. J., 2005. Dissolved inorganic phosphorous export to the coastal zone: results from a new, spatially explicit, global model (NEWS-SRP). Global Biogeochem. Cycles 19, GB4S03.
Hashimoto, K., Uchida, H., Nishimura, T., Oikawa, H., Funaki, H., Honma, C., et al., 2021. Determination of optimal culture conditions for toxin production by *Prorocentrum lima* complex strain with high diarrhetic shellfish toxins yield, 103, 102025.
Heil, C.A., Glibert, P.M., Fan, C., 2005. *Prorocentrum minimum* (Pavillard) schiller: a review of a harmful algal bloom species of growing worldwide importance. Harmful Algae 4, 449–470.
Hersbach, H., Bell, B., Berrisford, P., Hirahara, S., Horányi, S., Muñoz-Sabater, J., et al., 2020. The ERA5 global reanalysis. Q. J. Roy. Meteorol. Soc. 146, 1999–2049.
Hoppenrath, M., Chomérat, N., Horiguchi, T., Schweikert, M., Nagahama, Y., Murray, S., 2013. Taxonomy and phylogeny of the benthic *Prorocentrum* species (Dinophyceae) – a proposal and review. Harmful Algae 27, 1–28.
Hu, T., Curtis, J.M., Walter, J.A., McLachlan, J.L., Wright, J.L.C., 1995. Two new water-soluble DSP toxin derivatives from the dinoflagellate *Prorocentrum maculosum*: possible storage and excretion products. Tetrahedron Lett. 36, 9273–9276.
IOC, SCOR, IAPSO, 2010. The international thermodynamic equation of seawater - 2010: Calculation and use of thermodynamic properties, Manual and Guides No. 56, Intergovernmental Oceanographic Commission, UNESCO (English). available from. http://www.TEOS-10.org.
Jeong, H.J., Yoo, Y.D., Kim, J.S., Seong, K.A., Kang, N.S., Kim, T.H., 2010. Growth, feeding and ecological roles of the mixotrophic and heterotrophic dinoflagellates in marine planktonic food webs. Ocean Sci. J. 45, 65–91.
Kalnay, E., Kanamitsu, M., Kistler, R., Collins, W., Deaven, D., Gandin, L., et al., 1996. The NCEP/NCAR 40-year reanalysis project. Bull. Ame. Meteorol. Soc. 77, 437–472. https://doi.org/10.1175/1520-0477.
Karentz, D., Smayda, T.J., 1984. Temperature and the seasonal occurrence pattern of 30 dominant phytoplankton species in Narragansett Bay over a 22-year period (1959–1980). Mar. Ecol. Prog. Ser. 18, 277–293.
Karentz, D., Smayda, T.J., 1998. Temporal patterns and variations in phytoplankton community organization and abundance in Narragansett Bay during 1959–1980. J. Plankton Res. 20, 145–168.
Kattner, G., Becker, H., 1991. Nutrients and organic nitrogenous compounds in the marginal ice zone of the Fram Strait. J. Mar. Syst. 2, 385–394.
Koike, K., Sato, S., Yamaji, M., Nagahama, Y., Kotani, Y., Ogata, T., et al., 1998. Occurrence of okadaic acid-producing *Prorocentrum lima* on the Sanriku coast, Northern Japan. Toxicon 36, 2039–2042.
León-Muñoz, J., Urbina, M.A., Garreaud, R., Iriarte, J.L., 2018. Hydroclimatic conditions trigger record harmful algal bloom in western Patagonia (summer 2016). Sci. Rep. 8, 1330.
Li, W.K.W., 1980. Temperature adaptation in phytoplankton; cellular and photosynthetic characteristics. In: Falkowski, P.G. (Ed.), Primary Productivity in the Sea. Plenum Press, New York, USA, pp. 259–279.
Li, C., Weeks, E., 2009. Measurements of a small scale eddy at a tidal inlet using an unmanned automated boat. J. Mar. Syst. 75, 150–162.
Li, M., Ni, W., Zhang, F., Glibert, P.M., Lin, C.-H., 2020. Climate-induced interannual variability and projected change of two harmful algal bloom taxa in Chesapeake Bay, USA. Sci. Total Environ. 744, 140947.
Li, P.-F., Gao, P.-P., Liu, C.-Y., Zhang, H.-H., Yang, G.-P., 2021. Production of dimethyl sulfide and acrylic acid from dissolved dimethylsulfoniopropionate during the growth of *Prorocentrum minimum*. J. Appl. Phycol. 34, 219–230.
Lin, J.N., Yan, T., Zhang, Q.C., Wang, Y.F., Liu, Q., Zhou, M.J., 2014. *In situ* detrimental impacts of *Prorocentrum donghaiense* blooms on zooplankton in the East China Sea. Mar. Pollut. Bull. 88, 302–310.
Linford, P., Pérez-Santos, I., Montero, P., Díaz, P., Aracena, C., Pinilla, E., et al., 2023. Oceanographic processes favoring deoxygenation inside Patagonian fjords. EGUsphere. https://doi.org/10.5194/egusphere-2023-706 [preprint].
Longhurst, A., 1998. Ecological Geography of the Sea. San Diego Academic Press.
Loranzo-Duque, Y., Vidal, L.F., Navas, G.R., 2011. Lista de especies de dinoflagelados (Dinophyta) registrados en el mar Caribe colombiano. Boletín de Investigaciones Marinas y Costeras 40, 361–380.
Lovegrove, T., 1960. An improved form of sedimentation apparatus for use with an inverted microscope. Journal du Conseil Permanent International pour l'Exploration de la Mer 25, 279–284.
Lu, D., Jeanette, G., 2001. Five red tide species of the genus *Prorocentrum* including the description of *Prorocentrum donghaiense* Lu sp. Nov. from the East China Sea. J. Oceanol. Limnol. 19, 337–344.
Mancena-Pineda, J.E., Montalvo-Talaigua, M., Gavio, B., 2014. Potentially toxic dinoflagellates associated to drift in San Andres Island, international biosphere reservation-sea flower. Caldasia 36, 139–156.
Mardones, J.I., Clément, A., 2016. Manual de microalgas del sur de Chile. Puerto Varas, Chile.
Mardones, J.I., Paredes-Mella, J., Flores-Leñero, A., Yarimuzu, K., Godoy, M., Cascales, E., et al., 2023. Extreme harmful algal blooms, climate change, and potential risk of eutrophication in Patagonian fjords: insights from an exceptional *Heterosigma akashiwo* fish-killing event. Prog. Oceanogr. 210, 102921.
Marquet, P.A., Buschmann, A.H., Corcoran, D., Díaz, P.A., Fuentes-Castillo, T., Garreaud, R., et al., 2023. Global change and acceleration of anthropic pressures on Patagonian ecosystems. In: Castilla, J.C., Armesto, J.J., Martínez-Harms, M.J.,

Tecklin, D. (Eds.), Conservation in Chilean Patagonia. 19. Integrated Science, Springer, Cham, pp. 33–65.
McCullagh, P., Nelder, J., 1989. Generalized Linear Models., 2nd edn.(Chapman and Hall: London). Standard Book on Generalized Linear Models.
Mishra, S., Mishra, D.R., 2012. Normalized difference chlorophyll index: a novel model for remote estimation of chlorophyll-a concentration in turbid productive waters. Remote Sens. Environ. 117, 394–406.
Moreira-González, A.A., Fernandes, L.F., Uchida, H., Uesugi, A., Suzuki, T., Chomérat, N., et al., 2019. Variations in morphology, growth, and toxicity among strains of the *Prorocentrum lima* species complex isolated from Cuba and Brazil. J. Appl. Phycol. 31, 519–532.
Nascimento, S.M., Salguerio, F., Menezes, M., FA, Oliveira d, Nagalhães, V.C.P., De Pauala, J.C., et al., 2016. *Prorocentrum lima* from the South Atlantic: morphological, molecular and toxicological characterization. Harmful Algae 57, 39–48.
Ndhlovu, A., Dhar, N., Grag, N., Xuma, T., Picher, G.C., Sym, S.D., et al., 2017. A red tide forming dinoflagellate *Prorocentrum triestinum*: identifican, phylogeny and impacts on St Helena bay, South Africa. Phycologia 56, 649–665.
Nishimura, T., Uchida, H., Noguchi, R., Oikawa, H., Suzuki, T., Funaki, H., et al., 2020a. Abundance of the benthic dinoflagellate *Prorocentrum* and the diversity, distribution, and diarrhetic shellfish toxin production of *Porocentrum lima*. Harmful Algae 96, 101687.
Nishimura, T., Uchida, H., Suzuki, T., Tawong, W., Abe, S., Arimitsu, S., et al., 2020b. First report of okadaic acid production of a benthic dinoflagellate *Prorocentrum* cf *fukuyoi* from Japan. Phycol. Res. 68, 30–40.
Okolodkov, Y.B., 2005. The global distributional patterns of toxic, bloom dinoflagellates recorded from the Eurasian Arctic. Harmful Algae 4, 351–369.
O'Reilly, J.E., Werdell, P.J., 2019. Chlorophyll algorithms for ocean color sensors-OC4, OC5 & OC6. Remote Sens. Environ. 229, 32–47.
Pahleva, N., Smith, B., Schalles, J., Binding, C., Cao, Z., Ma, R., et al., 2020. Seamless retrievals of chlorophyll-a from Sentinel-2 (MSI) and Sentinel-3 (OLCI) in inland and coastal waters: a machine-learning approach. Remote Sens. Environ. 240, 111604.
Pei, L., Hu, W., Wang, P., Kang, J., Mohamed, H.F., Wang, C., et al., 2022. Morphological and phylogenic characterization of two bloom-forming planktonic *Prorocenrtum* (Dinophycea) species and their potential distribution in the China Sea. Algal Res. 66, 102788.
Pérez-Santos, I., Díaz, P.A., Silva, N., Garreaud, R., Montero, P., Henríquez-Castillo, C., et al., 2021. Oceanography time series reveals annual asynchrony input between oceanic and estuarine waters in Patagonian fjords. Sci. Total Environ. 798, 149241.
Pickard, G.L., 1971. Some physical oceanographic features of inlets of Chile. J. Fish. Res. Board Canada 28, 1077–1106.
Pingree, R.D., 1978. The formation of the shambles and other banks by tidal stirring of the seas. J. Mar. Biol. Assoc. U. K. 58, 211–226.
Pitcher, G.C., Figueiras, F.G., Hickey, B.M., Moita, M.T., 2010. The physical oceanography of upwelling systems and the development of harmful algal blooms. Prog. Oceanogr. 85, 5–32.
Polvani, L.M., Waugh, D.W., Correa, G.J., Son, S.W., 2011. Stratospheric ozone depletion: the main driver of twentiethcentury atmospheric circulation changes in the Southern Hemisphere. J. Climate 24, 795–812.
Quin, Q., Shen, J., 2019. Physical transport processes affect the origins of harmful algal blooms in estuaries. Harmful Algae 84, 210–221.
Quiñones, R.A., Fuentes, M., Montes, R.M., Soto, D., León-Muñoz, J., 2019. Environmental issues in Chilean salmon farming: a review. Rev. Aquac. 11, 375–402.
Reche, P., Artal, O., Pinilla, E., Ruiz, C., Venegas, O., Arriagada, A., et al., 2021. CHONOS: oceanographic information website for Chilean Patagonia. Ocean Coast. Manag. 208, 105634.
Reguera, B., Riobó, P., Rodríguez, F., Díaz, P.A., Pizarro, G., Paz, B., et al., 2014. *Dinophysis* toxins: causative organisms, distribution and fate in shellfish. Mar. Drugs 12, 394–461.
Rhodes, L.L., O'Kelly, H.J.A., 1994. Comparison of growth characteristics of New Zealand isolates of the prymnesiophytes *Chrysochromulina quadrikonta* and *C. camella* with those of the ichthyotoxic species *C. polylepis*. J. Plankton Res. 16, 69–82.
Robinson, I.S., 1981. Tidal vorticity and residual circulation. Deep-Sea Res. I (28), 195–212.
Rodríguez, E.A., Mancera, J.E., Gavio, B., 2010. Survey of benthic dinoflagellates associated to beds of *Thalassia testudium* in San Andrés Isla, Sewaflower Bisophere Reserve, Caribbean Columbia. Acta Biol. Colomb. 15, 229–246.
Rosales, S.A., Díaz, P.A., Muñoz, P., Álvarez, G., 2024. Modeling the dynamics of harmful algal bloom events in two bays from the northern Chilean upwelling system. Harmful Algae 132, 102583.
Rozzi, R., Rosenfled, S., Armesto, J.J., Mansilla, A., Nunez-Avila, M., Massardo, F., 2023. Ecological connections across the marine-terrestrial interface in Chilean Patagonia. In: Castilla, J.C., Armesto, J.J., Martínez-Harms, M.J., Tecklin, D. (Eds.), Conservation in Chilean Patagonia: Assessing the State of Knowledge, Opportunities, and Challenges. Springer Nature Switzerland AG, pp. 323–354.
Ruiz, C., Artal, O., Pinilla, E., Sepúlveda, H.H., 2021. Stratification and mixing in the Chilean Inland Sea using an operational model. Ocean Model. 158, 101750.
Sánchez, G.E., Pantoja, S., Lange, C.B., González, H.E., Daneri, G., 2008. Seasonal changes in particulate biogenic and lithogenic silica in the upwelling system off Concepcíon (~36S), Chile, and their relationship to fluctuations in marine productivity and continental input. Cont. Shelf Res. 28, 2594–2600.
Sarmiento, J.L., Gruber, N., Brzezinski, M.A., Dunne, J.P., 2004. High-latitude controls of thermocline nutrients and low latitude biological productivity. Nature 426, 56–60.
Schlitzer, R., 2015. Data analysis and visualization with ocean data view. CMOS Bulletin SCMO 41, 9–13.
Schneider, W., Pérez-Santos, I., Ross, L., Bravo, L., Seguel, R., Hernández, F., 2014. On the hydrography of Puyuhuapi Channel, Chilean Patagonia. Prog. Oceanogr. 128, 8–18.
Signell, R.P., Geyer, W.R., 1991. Transient eddy formation around headlands. J. Geophys. Res. - Oceans 96, 2561–2575.
Silva, N., Vargas, C., 2014. Hypoxia in Chilean Patagonian fjords. Prog. Oceanogr. 129, 62–74.
Silva, N., Sievers, H., Prado, R., 1995. Características oceanográficas y una proposición de circulación, para algunos canales australes de Chile entre 41°20'S y 46°40'S. Rev. Biol. Mar. 30, 207–254.
Strub, P.T., James, C., Montecino, V., Rutllant, J.A., Blanco, J.L., 2019. Ocean circulation along the southern Chile transition region (38°–46°S): mean, seasonal and interannual variability, with a focus on 2014–2016. Prog. Oceanogr. 172, 159–198.
Tomas, C., 1997. Identifying Marine Phytoplankton. Academic Press, Florida.
Trainer, V.L., Hickey, B., Horner, R., 2002. Biological and physical dynamics of domoic acid production off the Washington coast. Limnol. Oceanogr. 47, 1438–1446.
Utermöhl, H., 1958. Zur Vervollkomnung der quantitativen phytoplankton-Methodik. Mitteilungen – Internationale Vereinigung für Theoretische und Angewandte Limnologie 9, 1–38.
Venables, W.N., Ripley, B.D., 2013. Modern Applied Statistics with S-PLUS. Springer Science & Business Media, New York, USA.
Wells, M.L., Trainer, V.L., Smayda, T.J., Karlson, B.S., Trick, C.G., Kudela, R.M., et al., 2015. Harmful algal blooms and climate change: learning from the past and present to forecast the future. Harmful Algae 49, 68–93.
Wells, M.L., Karlson, B., Wulff, A., Kudela, R., Trick, C., Asnaghi, V., et al., 2020. Future HAB science: directions and challenges in a changing climate. Harmful Algae 91, 101632.
Yang, Z., Wang, T., 2013. Tidal residual eddies and their effect on water exchange in Puget Sound. Ocean Dyn. 63, 995–1009.
Zhang, J., Li, X., Wang, X., Guan, W., 2022. Transcriptome analysis of two bloom-forming *Prorocentrum* species reveals physiological changes related to light and temperature. Harmful Algae 125, 102421.
Zimmerman, J.T.F., 1978. Topographic generation of residual circulation by oscillatory (tidal) currents. Geophys. Astrophys. Fluid Dyn. 11, 35–47.
Zimmerman, J.T.F., 1981. Dynamics, diffusion and geomorphological significance of tidal residual eddies. Nature 290, 549–555.